UNIVERSITY OF BATH

Citation for published version:
Moroney, KM, Cronin, P, Adeleye, OA, Schaller, BE, Howard, MA, Castro-Dominguez, B, Ramachandran, R & Walker, GM 2020, 'An evaluation of the Johanson model for roller compaction process development for a high dose API', *Powder Technology*, vol. 366, pp. 82-95. https://doi.org/10.1016/j.powtec.2020.02.058

DOI:
10.1016/j.powtec.2020.02.058

Publication date:
2020

Document Version
Version created as part of publication process; publisher's layout; not normally made publicly available

Link to publication

Publisher Rights
CC BY-NC-ND

University of Bath

Alternative formats
If you require this document in an alternative format, please contact:
openaccess@bath.ac.uk

General rights
Copyright and moral rights for the publications made accessible in the public portal are retained by the authors and/or other copyright owners and it is a condition of accessing publications that users recognise and abide by the legal requirements associated with these rights.

Take down policy
If you believe that this document breaches copyright please contact us providing details, and we will remove access to the work immediately and investigate your claim.

Download date: 17. Jul. 2021

Journal Pre-proof

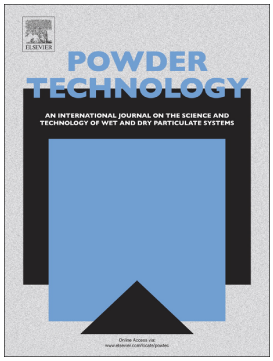

An evaluation of the Johanson model for roller compaction process development for a high dose API

Kevin M. Moroney, Patrick Cronin, Opeyemi A. Adeleye, Barbara E. Schaller, Matthew A. Howard, Bernardo Castro-Dominguez, Rohit Ramachandran, Gavin M. Walker

PII: S0032-5910(20)30164-9

DOI: https://doi.org/10.1016/j.powtec.2020.02.058

Reference: PTEC 15217

To appear in: *Powder Technology*

Received date: 19 November 2019

Revised date: 17 February 2020

Accepted date: 22 February 2020

Please cite this article as: K.M. Moroney, P. Cronin, O.A. Adeleye, et al., An evaluation of the Johanson model for roller compaction process development for a high dose API, *Powder Technology*(2020), https://doi.org/10.1016/j.powtec.2020.02.058

This is a PDF file of an article that has undergone enhancements after acceptance, such as the addition of a cover page and metadata, and formatting for readability, but it is not yet the definitive version of record. This version will undergo additional copyediting, typesetting and review before it is published in its final form, but we are providing this version to give early visibility of the article. Please note that, during the production process, errors may be discovered which could affect the content, and all legal disclaimers that apply to the journal pertain.

© 2020 Published by Elsevier.

Journal Pre-proof

An evaluation of the Johanson model for roller compaction process development for a high dose API

Kevin M. Moroney[a,b,*] kevin.moroney@ul.ie, Patrick Cronin[a], Opeyemi A. Adeleye[a], Barbara E. Schaller[a], Matthew A. Howard[d], Bernardo Castro-Dominguez[e], Rohit Ramachandran[f], Gavin M. Walker[c,a]

[a]*Synthesis and Solid State Pharmaceutical Centre (SSPC), Bernal Institute, University of Limerick, Ireland.*

[b]*MACSI, Department of Mathematics and Statistics, University of Limerick, Ireland.*

[c]*Department of Chemical Sciences, University of Limerick, Ireland.*

[d]*Johnson & Johnson Consumer, Inc., Fort Washington, PA, USA.*

[e]*Chemical Engineering Department, University of Bath, Cloverton Down, BA2 7AY Bath, United Kingdom.*

[f]*Dept.of Chemical & Biochemical Engineering, Rutgers, The State University of New Jersey, Piscataway, NJ 08854, USA.*

[*]Corresponding author.

Abstract

Roller compaction (RC) is a dry granulation technique applied to improve the flow and compressibility of drug formulations. RC implementation for high drug load formulations can be challenging due to flow issues and a high consumption of active pharmaceutical ingredient (API) for robust process development. This work addresses these challenges using process modelling for design and scale-up of an RC process on the same equipment and transfer to different equipment. A modified application of existing models incorporating a new description of mass transport in the feed screw is evaluated for guaifenesin formulations with a 90% drug loading. The model is

Abbreviations: API, active pharmaceutical ingredient; GFN, guaifenisen; MCC, microcrystalline cellulose PH102; MgSt, magnesium stearate; SiO_2, silicon dioxide; FT4, FT4 powder rheometer; CBD, conditioned bulk density; FEM, finite element method; DPC, Drucker-Prager Cap; OSD, oral solid dosage form; RC, roller compaction; DC, direct compression; WG, wet granulation; QbD, quality by design; RMSE, root mean squared error; NRMSE, normalised root mean squared error; FMRC, Vector Freund TF Mini roller compactor; BRC25, Bohles BRC25 roller compactor.

calibrated using low-throughput data on a Vector Freund TF Mini RC and used to predict ribbon density and throughput for various process settings at high-throughput. It is found that the modelling framework can reasonably predict high-throughput behaviour on the same RC but the predictive performance decreases for transfer between equipment.

Keywords: Roller compaction, Dry granulation, Pharmaceutical process modelling, Johanson model, High dose API, Ribbon density

Abbreviations:

API, active pharmaceutical ingredient; GFN, guaifenisen; MCC, microcrystalline cellulose PH102; MgSt, magnesium stearate; SiO_2, silicon dioxide; FT4, FT4 powder rheometer; CBD, conditioned bulk density; FEM, finite element method; DPC, Drucker-Prager Cap; OSD, oral solid dosage form; RC, roller compaction; DC, direct compression; WG, wet granulation; QbD, quality by design; RMSE, root mean squared error; NRMSE, normalised root mean squared error; FMRC, Vector Freund TF Mini roller compactor; BRC25, Robes BRC25 roller compactor.

1. Introduction

Roller compaction (RC) is increasingly being used in dry granulation processes during the manufacture of oral solid dosage forms (OSDs) in the pharmaceutical industry [1, 2]. It is usually deployed to improve poor flow and compressibility properties of the formulation, which make direct compression (DC) infeasible. This is achieved by size enlargement of the particles and an increase of the formulation bulk density [3]. In comparison to wet granulation (WG), dry granulation (DG) eliminates the requirement for a solvent or drying step making it particularly useful for heat or moisture sensitive active pharmaceutical ingredients (APIs) [4, 5]. RC also offers a shorter processing time and lower capital costs compared to WG for continuous manufacturing lines. Despite these advantages, developing a robust RC process is often more challenging than wet granulation [5]. In particular, while RC is used to improve the powder flowability, very poor flow of the initial formulation makes the process challenging [6]. It is also widely reported in the literature that granulation by RC can lead to a reduced performance of the formulation in terms of its compactibility and tabletability [7, 8].

In recent years, there is an increased demand in industry to develop OSDs with higher drug loads for applications where a high dose is needed. This is partially driven by patient issues such as the difficulty in swallowing large tablets. These tablets are necessary when a high dose is needed

but the percentage drug loading is low due to manufacturing challenges. High drug load OSDs are also more efficient in terms of limiting excipient use and lowering transport and storage costs. This presents a significant challenge for roller compaction, as RC formulations generally require higher amounts of excipient usage than WG. The increasing drug load means the API properties are expected to dominate the behaviour of the blended formulations [9, 10]. This phenomenon has been widely studied using percolation models [10, 11, 12]. Thus, for processes sensitive to blend flowability such as DC and RC there is a lower ceiling of drug load [10]. This challenge is emphasised in Leane et al. [11], where a comprehensive industry survey shows that for high dose formulations with a small particle size, over 80% are manufactured using WG. In the context of RC, we follow Reynolds et al. [13] by defining a high drug load to be a formulation having a mass fraction of API greater than 30%.

In order to follow a quality by design (QbD) approach, certain critical quality attributes (CQAs) need to be maintained through process development, testing, scale-up and technology transfer. For RC, the envelope density of the compacted ribbons has been widely selected as one of the CQAs [14, 15] and has been shown to be directly linked to the mechanical properties of the material [13]. In order to fully explore the process design space, expensive and labour-intensive experimental trials are often required, covering different throughputs and even transfer between different equipment [4, 16]. These challenges are amplified with a very high drug load. In the early stages of drug product development the API is often expensive to produce and available in limited quantities. This challenge is addressed by either using a model compound with similar properties to the API or trying to gain maximum information on low-throughput experiments [16]. Both approaches have significant challenges. In particular, process behaviour arises as a result of multivariate interactions between raw material properties and process parameters [17]. It is difficult to ensure that the fundamental properties driving the process variability can be extracted from experiments. Thus, it is not surprising that process design and scale-up is often done using a trial-and-error approach [18].

In RC, scale-up of material throughput can be achieved by increasing roll width, roll diameter, roll gap or roll speed. Process modelling approaches in recently published work [13, 19, 16], adapt the roller compaction model of Johanson [20] to develop a systematic approach to RC process development and scale-up throughput by roll width [13], roll diameter [19] and roll speed [16]. Each study shows promising results. In particular, the approach in ref. [16] involved model

calibration for low-throughput data and verified the prediction by comparing to experiments at high-throughput for an ibuprofen formulation of approximately 50% loading by mass. To the knowledge of the authors, this is the highest reported API loading in the literature which applies a variation of the Johanson modelling approach. Most studies consider either excipient mixtures ([21, 6]) or low API loads ($< 30\%$) ([22, 23, 24, 19]).

In this paper, we address a gap in the literature, by applying a process modelling approach to scale-up an RC formulation with a very high drug load (90%) from low-throughput to high-throughput on a single roller compactor. We also assess the accuracy of the developed model to transfer to a different roller compactor with a larger roll diameter. This is the first time a process modelling approach to scale-up from low to high-throughput has been presented in the literature for such a high drug loading of API. We present a new modified approach based on recently published work [13, 16] to address this challenge for an industrially relevant formulation of the API guaifenesin, which exhibits very poor flow behaviour, at 90% drug load. At this drug loading it is difficult to alter the poor flow behaviour of the API. A new description of the flow behaviour of the formulation in the feeding screw is proposed to account for the observed variations with process parameters.

α	nip angle
δ	angle of internal friction
$\dot{m}_s$	mass flow rate from screw
$\dot{m}_r$	mass flow rate from rolls
ff_c	flow function coefficient
γ	relative density or solid fraction
γ_0	relative density at the reference pressure
γ_r	ribbon relative density
μ	angle of inclination of the slip planes to the minor principal plane in the slip region
ω	angle measured anti-clockwise from the x-plane to the major principal plane
ϕ_w	wall friction angle
ρ_T	formulation true density

Journal Pre-proof

ρ_{app}	apparent compact density for uniaxial compaction
ρ_e	ribbon envelope density
σ	mean stress
σ_0	mean stress at entry to slip region
θ	angular roll position measured from the minimum gap
θ_h	entry angle into slip region
C	angle defined in equation (7)
C^*	cohesion
C_p	percent compressibility
c_s	screw constant or function
c_{s0}	screw function intercept
c_{s1}	screw function slope
D	roll diameter
D_T	compact diameter for uniaxial compaction
F	roll force factor
h	compact thickness for uniaxial compaction
K	compressibility constant
m	compact mass for uniaxial compaction
N_r	roll speed
N_s	screw speed
P	roll separating pressure
P_0	entry pressure
P_{max}	peak roll separating pressure
P_{ref}	reference pressure
R_f	roll force
R_p	roll pressure
S	roll gap

Journal Pre-proof

V_i powder volume before compression (compressibility test)

V_p compressed powder volume (compressibility test)

W roll width

x distance along the centre line between the rolls from the entry to the slip region

2. Modelling of roller compaction

In a recent publication, Toson et al. [16] combined the modelling approaches for roller compaction in refs. [20, 13], to present a model based approach for design and scale-up of a roller compaction process. The model was calibrated on data from experiments performed with a low material flow-rate (low-throughput) and used to predict the design space for a high material flow-rate (high-throughput) for two formulations containing approximately 50% ibuprofen. In this study, we present a similar approach which has been adapted to address the challenges of dealing with a very poor flowing API, guaifenesin at a very high loading of 90%.

2.1. Operating principles, key variables and modelling approaches

In the RC unit operation, blended powders are fed into a hopper and undergo dry granulation in a roller compactor. During roller compaction, powder is gravity-fed or screw-fed into the gap between a set of counter rotating rolls. Once the powder is between the rolls, it is conveyed by friction between the material and the roll surfaces, through the gap between them. At the point of minimum gap it undergoes compression under high stresses and forms a compacted ribbon. There is a large variety of different roller compactor designs which are discussed in detail in refs. [25, 26, 27]. The ribbons are subsequently milled into granules. Roller compaction is a conceptually simple process [28] but a lack of understanding of the mechanisms of compaction mean that it is difficult to produce ribbons of the required characteristics [25]. The space between the rolls is generally divided into three regions called the slip region, the nip region and the release region. The regions are shown in figure 1.

Figure 1: Schematic of a screw-fed roller compactor. The diagram shows a top-fed orientation, with hopper, feed screw and compacting rolls, but the screw may be inclined at different angles.

Three regions, namely the slip, nip and release regions, are marked. The x-coordinate points into the slip region with $x = 0$ at the entry. The entry angle $\theta = \theta_h$ and the nip angle $\theta = \alpha$ are shown.

The boundaries between the regions are described by their angular position from the minimum gap between the rolls. The slip region is characterised by the particles slipping off the surfaces of the rolls. The powder behaviour in this region is mainly determined by the friction between the powder and the walls and the internal powder friction. The entry to this region is defined by the entry angle θ_h. The nip region begins at the nip angle α, where the stress normal to the roll surface becomes large enough that the rolls can "grip" the powder. At this point, the powder velocity at the roll surface becomes equal to the roll velocity. The main compaction occurs in the nip region, as powder is dragged through the minimum roll separation. The normal stress on the rolls increases dramatically reaching its maximum value at the neutral angle, which does not necessarily correspond to the angle at the smallest gap [28]. The release region starts beyond the neutral angle, as the gap between the rolls begins to increase again. While many papers, such as early work by Johanson [20], assume that the maximum pressure occurs at the minimum gap between the rolls, more recent work by Cunningham and others, shows the maximum pressure occurs prior to the minimum gap [22, 30, 31, 21, 6]. The compacted ribbon may increase in size somewhat compared to the minimum roll separation due to elastic recovery in the release region. The compacted material may move faster than the rolls in the release region and slip between the ribbon and the rolls may again occur.

The main aim of the roller compactor is to achieve compacted ribbons with a target density (or porosity) at a given mass-throughput. The feasibility of achieving these targets depends on the material properties, the roller compactor design and configuration and the operating settings. The main design variables which influence roller compactor performance include roll configuration (see ref. [28] for examples), roll diameter D, roll width W, roll surface finish (smooth or grooved etc.) and feeding system. There are a wide range of operating parameters which can influence material throughput and final ribbon density. These include roll pressure (roll force R_f), screw speed N_s, roll speed N_r and roll gap S. There are two major operating modes [13, 16]:

- Gap-controlled mode: The roll speed, roll force and gap width are set. An internal

feedback control system is used to vary the screw speed to correct for any variations in roll gap to keep it at its set point.

- Screw-controlled mode: The roll speed, roll force and screw speed are fixed. The resulting roll gap arises from the interaction of these parameters and the material properties of the formulation.

When scaling-up the RC process, or transferring between equipment with different design parameters, it is important to have a quantitative understanding of the influence of each of these parameters on the target variables. For different control modes, variations of Johanson's model (gap-controlled) and Reynolds' model (screw-controlled) can be applied [16].

Johanson's model and its recent extensions by Reynolds [16] and Toson et al. [16] are limited by the assumptions of 1-dimensional flow and compaction and a very simple material law. These limitations will be considered in section 2.3.7. For this reason, a variety of other models have been applied to describe RC. The 'slab' model was developed by Katashinskii [32] and has been well described recently by refs. [31, 29]. The model considers plane strain, similar to that of Johanson's approach, with an equilibrium force balance being formed on trapezoidal slabs of differential thickness in the nip region. The equations are supplemented with constitutive relationships for the friction behaviour at the roll surface, the yield surface and the densification behaviour to close the system. Examples can be found in refs. [31, 33, 29]. More complex continuum models have been developed to solve for the 2- or 3-dimensional stress and velocity fields and density distributions between the rolls. Most of these works use the density dependent Drucker-Prager Cap model and are solved using finite element methods (FEM) in the ABAQUS® software [31, 29, 30, 34, 35, 36, 37, 38]. Recent work by Mazor et al. [39] applied the discrete element method (DEM) to produce a combined DEM-FEM model to investigate the influence of oscillations in the inlet stress on the density homogeneity of the produced ribbon. Advanced 3-dimensional FEM methods have also been used by Krok and Wu [40] to predict thermomechanical behaviour of the powder during compaction to resolve stress, density and temperature distributions. The application of sophisticated high fidelity models such as FEM and DEM is becoming more feasible with increased computation power. These models are also very useful to test the assumptions of 1-D models such as Johanson's and investigate phenomena such as oscillations in inlet stress, the influence of roll friction and the homogeneity of ribbon density. However, these methods are computationally expensive and require extensive experiments to

parametrise for each formulation, across a range of densities. The models can also be sensitive to experimental errors in parameter determination [41]. Thus, while FEM and DEM-FEM models are very useful for process understanding and visualisation and physically more realistic, approaches such as those in refs. [13, 22, 16] remain the most practical for process development.

2.2. Roller compactor throughput

The material throughput of a roller compactor is a key consideration for manufacturing. It can be predicted based on the assumption that the screw throughput $\dot{m}_s$ is linearly proportional to the screw speed N_s, so that

$$\dot{m}_s = c_s N_s, \tag{1}$$

where c_s is the screw constant representing the mass conveyed by one revolution of the screw. It is possible to fit the screw constant by running material through the screw uncoupled from the rolls at different speeds. However, this will over predict the screw constant during operation due to back pressure from the rolls [25]. Thus, it is better to fit c_s from data when the rolls are engaged. Throughput can also be predicted from the mass flow rate out of the rolls $\dot{m}_r$ given by

$$\dot{m}_r = \rho_T \gamma_r \pi DWSN_r, \tag{2}$$

where ρ_T is the formulation true density, γ_r is the ribbon relative density, N_r is the roll speed, D is the roll diameter, W is the roll width and S is the minimum roll gap between the rolls. In equilibrium operation, assuming there is no loss of material via side leakage, mass conservation requires $\dot{m}_s = \dot{m}_r$. Equating equations (1) and (2) gives

$$\rho_T \gamma_r \pi DWS = c_s \frac{N_s}{N_r}. \tag{3}$$

If a range of experiments are conducted in the design space recording all variables and responses in equation (3), then c_s can be determined. However, this assumes that the mass delivered per rotation of the screw does not depend on either the screw speed, or the back pressure generated by the rolls. It is commonly recognised that screw efficiency should decrease as the screw speed increases above some level [42]. Roberts [42] attributes this to a combination of a change of fill level (called fullness efficiency) and vortex efficiency, which relates to the rotational motion of powder within the screw. To account for this, we propose the following empirical screw mass

transfer rate to replace the screw constant

$$c_s = c_{s0} + c_{s1}\frac{N_s}{N_r}, \tag{4}$$

where c_{s0} and c_{s1} are constants to be determined. Choosing $c_{s1} = 0$ recovers the standard definition of the screw constant. We expect c_{s1} to be negative so the mass conveyed per revolution decreases as screw speed increases. For a fixed screw speed, increasing the roll speed increases the screw mass transfer rate. This accounts for a decreased back pressure on the screw from the rolls which may influence the slip condition between the screw and the powder. It should be clear that equation (4) is an empirical relationship and is only useful if it can capture the observed throughput. Also care should be taken if extrapolating outside of the range of N_s / N_r on which it is trained. Certainly, if the screw reaches a limiting mass flow rate, equation (4) will not hold.

In order to calibrate equation (4) at low-throughput, the roll speed can be fixed at its lower operating set point and the screw speed and roll force varied to cover the low and high points in the operating window. If the range of possible values of screw speed to roll speed ratio relevant to high throughput production can be covered, then it may be possible to predict these throughputs.

2.3. Roller compactor ribbon density

The first mechanistic model of roller compaction was proposed by Johanson [20]. A number of modifications to Johanson's model have been proposed to make it suitable for process design and scale-up [13, 22, 14, 38, 16] and in-process control [43, 44, 45]. For process design applications, the Johanson model has been well described in refs. [13, 22, 16]. The presentation here is similar but differs in some key aspects. Thus, the exact equations that are being solved and the associated assumptions are detailed in the following sections.

Johanson's original model did not account for the influence of screw speed or roll speed or the resulting throughput on compression behaviour for screw-controlled roller compactors. This has been addressed by ref. [13]. The original model also required the inlet stress on the powder in the feed region to be specified to solve the model. In practice, this is very challenging to measure. Following Reynolds [13], this issue is addressed in this study by using measured roll force as an input rather than feed pressure.

Journal Pre-proof

The Johanson model applies to the nip and slip regions in the roller compactor (see Figure 1). Any elastic recovery in the release region is not modelled. The coordinate system adopted is as shown in figure 1, with the x-axis in the direction of the flow.

2.3.1. Stress modelling in slip region

In the slip region, Johanson assumes plane stresses and strains (2-dimensional) and describes the stress state using Euler's equations for static equilibrium. This facilitates the analysis of stress via Mohr circles [46] with the Coulomb yield criterion being adopted.

Johanson combines the effective yield locus with Euler's equations for static equilibrium, giving a coupled system of hyperbolic partial differential equations describing the stress field in the slip region in terms of the mean pressure and an angle α, which is the angle measured anti-clockwise from the x-plane to the major principal plane. Based on some simplifying assumptions, an ordinary differential equation for the mean stress at the centreline between the rolls is derived. The details of this will not be outlined here, but can be found in [47, 20]. The entry angle to the slip region, denoted θ_h, is defined as the angle at which the major principal stress acts horizontally, which is given by (for $\phi_w \le \delta$)

$$\theta_h = \frac{1}{2}\left(\arcsin\left(\frac{\sin\phi_w}{\sin\delta}\right) + \phi_w\right). \tag{5}$$

Johanson's equation was initially written in the x-coordinate, representing distance along the centre line measured from the upper boundary of the slip zone. However, it is advantageous to write it in the θ-coordinate measuring the angular position measured from the minimum gap, using a simple change of variables. The ordinary differential equation for the mean stress at the centreline is

$$\frac{\mathrm{d}\sigma}{\mathrm{d}\theta} = -\frac{4\sigma\left(\theta_h - \theta\right)\tan\delta\cos\theta}{\left(1+\frac{S}{D}-\cos\theta\right)\left(\cot(C-\mu)-\cot(C+\mu)\right)}, \tag{6}$$

where

$$C = \frac{1}{2}\left(\pi - \theta_h + \theta\right), \mu = \frac{\pi}{4} - \frac{\delta}{2}. \tag{7}$$

Physically $\pm\mu$ represent the angles of inclination of the slip planes to minor principal plane. Given the entry pressure P_0 at $\theta = \theta_h$, the mean stress at the entry angle, σ_0, can be calculated as

$\sigma_0 = P_0/(1-\sin\delta)$ and equation (6) can be integrated numerically to give the mean stress at the centreline in the slip region.

2.3.2. Stress modelling in the nip region

The nip region beings at an angle α where the material begins to stick to the rolls. A simplified mass balance model is used here. The action of the roller compactor is approximated as 1-dimensional compression assuming that a narrow strip of material at the nip angle, must be compressed into a strip of the same thickness, with a width equal to the minimum roll gap. A constitutive relationship is required to relate the compact relative density γ to the stress level. The Johanson model uses a power law relationship given by

$$\sigma = C_1\gamma^K, \tag{8}$$

where C_1 and K are constants. The exponent K is related to the material's compressibility, where small K values indicate very compressible materials and large K values indicate incompressible materials. Care should be taken in measuring K, as it may depend on experimental conditions such as moisture content, temperature and time of compaction. The roll separating pressure (stress acting normal to the centreline) is of more practical importance. This is related to the mean stress by $P = \sigma(1+\sin\delta)$. The useful constitutive rule is:

$$P = P_{\text{ref}}\left(\frac{\gamma}{\gamma_0}\right)^K \quad \text{or} \quad \gamma = \gamma_0\left(\frac{P}{P_{\text{ref}}}\right)^{\frac{1}{K}}. \tag{9}$$

Commonly K is found by performing uniaxial compaction experiments and plotting the log of relative density against the log of applied pressure, but can also be fitted with non-linear regression techniques. Typically the pre-consolidation density γ_0 corresponds to the relative density at a reference pressure of 1Mpa. Combining mass balance and constitutive behaviour the expression for mean stress in the nip region at any angle θ is

$$\sigma_\theta = \sigma_\alpha\left(\frac{\left(1+\frac{S}{D}-\cos\alpha\right)\cos\alpha}{\left(1+\frac{S}{D}-\cos\theta\right)\cos\theta}\right)^K. \tag{10}$$

Given the mean stress at the nip angle, the stress at any angle in the nip region can be determined. This value can be got from solving for the stress distribution in the slip region and requiring

continuity of stress at the nip angle. Differentiating equation (10) yields the stress gradient in the nip region:

$$\frac{\mathrm{d}\sigma}{\mathrm{d}\theta} = K\sigma\left(\frac{1+\frac{S}{D}-2\cos\theta}{1+\frac{S}{D}-\cos\theta}\right)\tan\theta. \tag{11}$$

Equations (6) and (11) are commonly incorrectly written in the literature, where the rate of change of stress with angular coordinate θ is incorrectly equated to expression of rate of change of stress with the linear coordinate x originally presented by Johanson. Fortunately these errors cancel when calculating the nip angle, but lead to errors if the stress profile is calculated.

2.3.3. Estimation of nip angle

From equations (6) and (11) there are two differential equations describing the stress gradient at each point (one based on slip at the roll surface and one based on sticking.) Calculation of the stress at each point requires integration of one or other of these equations forward. Johanson carried out the integration by selecting the minimum gradient at each point in an upper bound type of argument [29]. This defines two regions: (i) the slip region where the gradient in (6) is smaller ($\alpha < \theta < \theta_h$) and (ii) the nip region where the gradient in (11) is smaller ($0 < \theta < \alpha$). The region $\theta < 0$ is not considered. The nip angle occurs at the angle α between the two regions where the stresses and the stress gradients are equal given by

$$\frac{4(\alpha-\theta_h)\tan\delta\cos\alpha}{\left(\cot(C-\mu)-\cot(C+\mu)\right)} = K\left(1+\frac{S}{D}-2\cos\alpha\right)\tan\alpha. \tag{12}$$

The nip angle depends on the parameters δ, ϕ_w and K and is largely independent of the roll geometry, provided $\frac{S}{D} \ll 1$. Once the nip angle has been calculated, the stress distribution between the rolls can be calculated in the slip and nip regions.

2.3.4. Calculation of ribbon density from roll force

The main utility of the Johanson model is that it gives key quantities of interest, such as the nip angle and the roll force, in terms of some basic material and equipment parameters. The roll force R_f can be related to the peak pressure $P_{\max}$ by integrating the roll separating pressure

$\sigma_\theta(1+\sin\delta)$ between the nip angle and the angle of minimum gap giving

$$R_f = \frac{P_{\max} WDF}{2}, \tag{13}$$

where

$$F = \int_{\theta=0}^{\theta=\alpha(\delta,\phi_w,K)} \left(\frac{\frac{S}{D}}{\left(1+\frac{S}{D}-\cos\theta\right)\cos\theta} \right)^K \cos\theta \mathrm{d}\theta. \tag{14}$$

This implicitly assumes the contributions of the pressure on the rolls in the slip region and the release region are negligible. Combining equations (9) and (13), gives a single equation for the output ribbon relative density (γ_r) in terms of the equipment and material parameters [13]

$$\gamma_r = \gamma_0 \left(\frac{2R_f}{WD\int_{\theta=0}^{\theta=\alpha(\delta,\phi_w,K)} \left(\frac{\frac{S}{D}}{\left(1+\frac{S}{D}-\cos\theta\right)\cos\theta} \right)^K \cos\theta \mathrm{d}\theta} \right)^{\frac{1}{K}}. \tag{15}$$

Note that the equation in this form requires the units of the bracketed term to be in MPa.

2.3.5. Ribbon density prediction in screw controlled mode

In gap-controlled roller compactors, such as the Bohles BRC25, the process set point of roll gap can be used in equation (15) to determine the ribbon density provided stable control can be achieved. In a screw controlled configuration, such as the Vector Freund TF Mini, the screw speed is set and the roll gap responds. In this case S depends on the process settings. This can be addressed by solving equation (3) for S and substituting into (15) to give

Journal Pre-proof

$$\gamma_r = \gamma_0 (2R_f)^{\frac{1}{K}} \left(WD \int_{\theta=0}^{\theta=\alpha(\delta,\phi_w,K)} \left(\frac{\left(c_{s0} + c_{s1} \frac{N_s}{N_r} \right) N_s}{\pi \rho_T \gamma_r W D^2 N_r \left(1 + \frac{\left(c_{s0} + c_{s1} \frac{N_s}{N_r} \right) N_s}{\pi \rho_T \gamma_R W D^2 N_r} - \cos\theta \right) \cos\theta} \right)^K \cos\theta \, \mathrm{d}\theta \right)^{-\frac{1}{K}} . \quad (16)$$

This expression is distinct from previous models in refs. [13, 22, 16] in the use of a non constant term for c_s as outlined in section 2.2. The substitution of S means it is not possible to solve explicitly for γ_r and equation (16) needs to be solved via an iterative root solving algorithm.

2.3.6. Model calibration and parameter estimation

The model parameters need to be estimated as accurately as possible, using the minimum material. Toson et al. [16] calibrate their models at low-throughput to reduce the material used. We adopt and extend this idea here. The Johanson and throughput models are semi-empirical so we cannot expect them to be valid outside the data they are trained on. The range of densities on which the model is trained should cover the range of densities on which the model is required to predict. Similarly, training of the screw function should cover as much as practical the range of values of N_s / N_r. The roll speed is set to the minimum value under consideration. In terms, of ribbon density the maximum value should be realised by setting the roll force to a maximum and the screw speed to the maximum, while setting both to the minimum will result in minimum ribbon density. Clearly using more points than this will lead to a more robust fit on the two parameters γ_0 and K. Varying the screw speed from the minimum value to the maximum will also give a range of N_s / N_r to calibrate the screw function. Performing these experiments at low roll speed, limits the throughput during model calibration.

Firstly we consider the calibration of a process development model on a screw controlled roller compactor. The factors considered are screw speed, roll speed, roll pressure (force) and silicon dioxide level. The feasible processing space is narrow and the range of screw speed and roll

speed values resulting in intact ribbons is strongly dependent on roll force. For this reason, standard full factorial or central composite designs were not possible. A non-standard design covering the feasible space and consisting of 27 runs was selected (see Section 4), with three levels of roll speed of 3, 5 and 7. Model calibration was performed on the 9 runs with $N_r = 3$. The model performance for prediction is assessed on the higher throughput runs.

Depending on the control mode, equation (15) or (16) can be used to predict ribbon density, once the material and process parameters are known. The parameters ρ_T, δ, ϕ_w can be determined experimentally while the equipment geometry and process settings are known. The challenge is to determine the values of γ_0 and K. While uniaxial compression provides a quick way to estimate these values, it is widely reported in the literature that this leads to an over-prediction of the relative density for given process settings [13]. An alternative approach is to perform a number of experiments at low-throughput (minimum of 2) and measure the ribbon density and record the process settings. This data can then be used to find the values of γ_0 and K that best fit equation (15) or (16) to the data. This is done using a non-linear least squares solver to minimise a given objective function. We choose to minimise the sum of the squared residuals between the model prediction and the data. An iterative solver is needed. The calibrated model can be used to predict the ribbon density at higher throughput. For the screw function, the value of c_s for each individual experiment can be calculated using equation (3). These values can then be used to fit the values of c_{s0} and c_{s1} in equation (4) using a linear regression model.

The steps in model calibration are as follows (see Figure 2):

1. Collect data for low-throughput experiments. This includes material properties (δ, ϕ_w, ρ_T), equipment geometry (D, W) and run setting and measurements (N_s, N_r, R_f, γ_r, S) for each experimental run.
2. Calculate c_s for each run using equation (3).
3. Fit c_{s0} and c_{s1} in equation (4) using a linear regression model.
4. Choose initial guesses for K and γ_0 (can be estimated from uniaxial compression data).
5. Estimation of K and γ_0 involves an iterative procedure until desired accuracy is

reached:

- Calculate entry angle and nip angle using equation (5) and (12).
- Substitute into equation (15) or equation (16) and solve for γ_r for each experiment. Calculate the sum of the squared residuals between the model ribbon density prediction and the experimental data points.
- If the desired accuracy is met the process is finished. If not, new values of γ_0 and K are selected by the algorithm and step 5 is repeated.

The model calibration is performed in MATLAB®. The linear regression to determine the screw function parameters is performed using the built-in function '`fitlm`' which uses an algorithm applying QR decomposition. The values of γ_0 and K are determined using the built-in non-linear regression function '`fitnlm`' which uses the Levenberg-Marquardt nonlinear least squares algorithm [48]. The simultaneous 95% confidence bands for the ribbon density true mean response are calculated using the '`predict`' function.

It is important to highlight that the primary roller compactor used in this study was not equipped to measure the in-process roll gap. Thus, in this work S is measured from the final ribbon thickness, which is typically larger than the actual roll gap due to elastic recovery. The model is easily adapted to include different values for roll gap and ribbon thickness by including an elastic recovery factor corresponding to the ratio of thickness to roll gap such as in ref. [16]. However, as the in-process roll gap is not recorded in this study, it is best to calibrate the model based on the predicted responses the density and thickness of the final ribbon.

2.3.7. Model limitations and criticisms

A number of criticisms of the Johanson model have been documented in the literature. In particular, Sommer et al. [49] criticise the method of estimation of nip angle for lacking a sound theoretical basis. The method of calculation of entry angle and linear dependence of maximum pressure on the entry stress is also criticised. The simple nature of the material law in the nip region is also questioned and highlighted as a key reason for discrepancies with experimental results. Cunningham [29] highlights the lack of modelling of elastic unloading and the release region. Liu et al. [38] highlight the errors due to the assumption of one dimensional flow in the nip region. This difficulty is emphasised by doing a 2-D FEM simulation of powder flow and compaction using the

Journal Pre-proof

DPC model. Based on this the assumption of one dimensional flow and mass balance is adjusted using a mass correction factor, which is a function of angular position. The extra degrees of freedom allow for a much better agreement with the FEM model. Nevertheless, this requires the FEM method to be parametrised for the material in question, requiring specialised instrumented equipment. The Johanson model is also unsuitable for incompressible material, where slip must occur on the roll surface meaning no nip region exists [50, 51, 5]. It is important to recognise these limitations when using the Johanson model and ensure it is suitable and properly calibrated for the application in question.

Figure 2: Flow chart for model development. The model is calibrated on low-throughput data ($N_r = 3$).

3. Materials and Methods

3.1. Formulation

Guaifenesin (GFN, supplied directly by Janssen) was chosen as a model API for this work. The formulation required a fixed API loading of 90 wt%. The remainder of the blend was made up of microcrystalline cellulose PH102 (MCC, Sanaq) as a primary excipient, a fixed quantity of 0.5 wt% magnesium stearate (MgSt, Faci S.P.A.) as a lubricant and varying amounts (0–0.5 wt%) of fumed silicon dioxide (SiO_2, Aerosil 200 Pharma, Evonik). The formulations studied are listed in Table 1.

Table 1: Formulation composition by mass percentage.

Formulation	Guaifenesin	MCC PH102	Magnesium Stearate	Silicon dioxide
F_0	90	9.5	0.5	0
$F_{0.1}$	90	9.4	0.5	0.1
$F_{0.3}$	90	9.2	0.5	0.3
$F_{0.5}$	90	9.0	0.5	0.5

3.2. Preparation of blends

Small batch blends for initial testing were prepared using a Caleva Multi-Lab mixer equipped with inter-meshing counter rotating blades at 60 rpm. The blends were prepared in the following order: GFN was pre-blended with the excipient MCC for a duration of 5 minutes. Silicon dioxide was added to this blend and mixed for 5 minutes (when used). Magnesium stearate was added last and mixed for one minute to avoid it fully coating the particles [52]. For larger quantities of blends (> 25g), a tumble mixer (Stuart STR4/3) was used with a set rotation speed of 30 rpm. The material was added into a two-litre container with a maximum fill level of 50% to ensure adequate mixing. The powders were always added in the same order and using the same mixing times. The procedure to ensure a well-mixed batch was determined based on an initial study. The improvement in flowability due to excipients initially increased with mixing time. The mixture was considered homogeneous when flowability no longer improved with increasing time and no particles were found adhered to the container.

3.3. Properties of individual powders and blends

3.3.1. Particle size analysis

The particle size distribution of individual powders and blends was determined using laser diffraction analyser (Microtrac S3500). The measurements were made in triplicate and the analysis method for irregular particle shape was used.

3.3.2. Bulk density

The conditioned bulk density (CBD) of all individual materials and blends was obtained as part of the compressibility test on the FT4 powder rheometer (Freeman Technology) which is described in section 3.3.4.

3.3.3. True density

The true density of individual powders was determined using a gas pycnometer (AccuPyc II 1340, Micromeritics) in a helium atmosphere. The true density ρ_{Tb} of the blended formulations was calculated from the mass fractions x_i and true densities ρ_{Ti} of the individual components.

In this study, true density is given by

$$\rho_{Tb} = \frac{1}{\sum_{i=1}^{4} \frac{x_i}{\rho_{Ti}}}, \tag{17}$$

where $i = 1, 2, 3, 4$ represent the individual powders.

3.3.4. Compressibility test

The compressibility test is a standard test procedure on the FT4 which measures the percentage volume change of a powder bed from its initial resting bulk volume before compression V_i, to its compressed volume V_p. The method is described in detail in [53]. The percent compressibility C_p is given by

$$C_p = \frac{100(V_i - V_p)}{V_i}. \tag{18}$$

Lower values of compressibility indicate an increased ability of the powder to flow from a low-stress state.

3.3.5. Shear cell test

The rotational shear cell test on the FT4 was used to determine the angle of internal friction δ, cohesion C^* and the flow function coefficient f_c of the individual materials and the blends. The test was performed using a pre-consolidation pressure of $9\,\text{kPa}$ as described by Wang et al. [54]. Higher values of f_c indicate an easier flow from a pre-stressed state.

3.3.6. Wall friction test

The wall friction angle ϕ_w is calculated using the rotational wall friction module on the FT4. The standard test method is used with a preshear stress of $9\,\text{kPa}$. Three 316 stainless steel discs with surface roughness values of $0.05\,\mu\text{m}$, $0.28\,\mu\text{m}$ and $1.2\,\mu\text{m}$ were used to assess the variation of wall friction angles of the blends. This compares to a value of $0.4\,\mu\text{m}$ used in previous studies, which applied ring shear testers rather than the cylindrical one on the FT4 [13, 55, 1]. The test involves preconditioning steps identical to that in shear cell test followed by

Journal Pre-proof

preshearing the sample at the shear stress σ_{ps}. The sample is consolidated to a fixed normal stress using the stainless steel plate. The plate is then rotated slowly at a fixed velocity. Shear failure will occur in the bed at some value of shear stress. The measured steady shear stress τ_{ps} is recorded. This test is repeated at a set of reducing normal stresses $\sigma_i, \sigma_{ii}, \ldots$ with the corresponding steady state shear stresses $\tau_i, \tau_{ii}, \ldots$ being recorded. The steady shear stress is calculated as the average of the values over the last 10% of the shearing time for each normal stress. The angle of wall friction is calculated from the slope of the wall yield locus produced by the points $\{(\sigma_{ps}, \tau_{ps}), (\sigma_i, \tau_i), (\sigma_{ii}, \tau_{ii}), \ldots\}$.

3.4. Uniaxial compaction properties

The compaction properties of the material in the nip region are described in the Johanson model by the compressibility factor (K) and the pre-consolidation relative density γ_0. These parameters can be estimated by uniaxial compression of the blends at a range of pressures to determine the pressure-relative density relationship. This analysis was performed on a compaction simulator (Gamlen Tableting D series) equipped with a 6 round and flat-faced punch and die set. The compaction was force controlled and compacts were made at a range of applied loads from 50 kg to 500 kg giving pressures from 17.34 MPa to 173.47 MPa covering the range of solid fractions relevant for roller compaction. Compaction velocity was set at $1\,\mathrm{mm\,s^{-1}}$. For each compression, 100 mg was manually weighed out and compacted in the die. The tablet dimensions were determined by caliper measurement and the tablet solid fraction γ calculated according to the equation

$$\gamma = \frac{\rho_{\mathrm{app}}}{\rho_T} = \frac{4m}{\rho_T \pi D_T^2 h}, \tag{19}$$

where m is the compact mass, D_T is the compact diameter, h is the thickness and ρ_{app} and ρ_T are the apparent tablet density and true density of the blend, respectively. Compacts were made in triplicate.

3.5. Roller compaction

Two roller compactors were used in this study. Model development and validation was performed on a Vector Freund TF Mini roller compactor (FMRC). The model was also evaluated on a Bohles BRC25 roller compactor. The FMRC was fitted with stainless steel rolls with a width of $25\,\text{mm}$ and diameter of $100\,\text{mm}$. The rolls are top-fed by a feed screw from a hopper. The applied hydraulic pressure can be varied to produce roll forces up to a maximum compression force of 48 kN. The roller compactor is instrumented to record roll force. The screw speed and roll speed can be set independently and the system is controlled to maintain a set roll pressure. Ribbons were manufactured at a range of screw speeds ($3-60\,\text{rpm}$), roll speeds ($3-7\,\text{rpm}$) and roll pressures ($0-20\,\text{bar}$). The BRC25 was equipped with stainless steel rolls with a width of $25\,\text{mm}$ and diameter of $250\,\text{mm}$. The system can operate up to a maximum specific compaction force of $20\,\text{kN cm}^{-1}$ giving it a maximum possible applied force of $50\,\text{kN}$ for the equipped rolls. The rolls are top-fed by a vertical tamping screw, which is fed from a hopper by a horizontal feed screw. Experiments on the BRC25 were performed by specifying the specific roll force, the roll speed and the target roll gap width. The tamp screw automatically adjusted to maintain the target roll gap. The feed screw automatically adjusts its speed in proportion with the tamp screw to maintain screw fill level. Experiments on the BRC25 were performed at a target roll gap of $1.5\,\text{mm}$, and roll speeds of 6 and $12\,\text{rpm}$, while specific roll force varied from $2\,\text{kN cm}^{-1}$ to $4.5\,\text{kN cm}^{-1}$.

3.6. Ribbon thickness and relative density measurements

Ribbon samples collected from various RC operations were analysed to determine their thickness and relative density (solid fraction). The ribbon thickness was determined using a digital callipers with measurements made in triplicate for each condition. The ribbon relative density was calculated as the ratio of the ribbon's envelope density ρ_e to its true density ρ_T. The true density was determined from equation (17). The envelope density was determined using the Geopyc envelope density analyser (Geopyc 1360, Micromeritics). Details on the envelope density measurement in the Geopyc are given in [15]. Measurements were made in triplicate.

3.7. Experimental design

A design of experiments (DoE) was implemented on the FMRC to investigate the influence of lubricant level (SiO_2 %), screw speed, roll speed and roll pressure (roll force). Three levels were

selected for each factor except screw speed. The feasible processing space where ribbons were produced did not allow for the same limits of screw speed to be used for different roll pressures. A non standard design comprising 27 runs was selected (see Table 2). A small number of runs were performed on the BRC25 with an SiO_2 level of 0.1%. The conditions for these runs are listed in Table 3. In the BRC25, the target roll gap is set, as is the specific compaction force. The actual compaction force is given here. The screw speed responds to keep the roll gap constant, in this case 1.5 mm. The average screw speed during operation for each condition is also given in the table.

Table 2: Experimental design on FMRC.

Run	N_s (rpm)	N_r (rpm)	SiO_2 (%)	R_p ( )	N_s / N_r (-)	R_f ( )
1	12	3	0.1	0	4	1.67
2	13	3	0.1	0	4.33	1.67
3	28	7	0.1	0	4	1.56
4	37	7	0.1	0	5.29	1.68
5	15	5	0.1	10	3	3.15
6	3	3	0.1	20	1	6.18
7	9	3	0.1	20	3	6.24
8	10	7	0.1	20	1.43	6.30
9	60	7	0.1	20	8.57	6.22
10	23	5	0.3	0	4.6	1.48
11	8	3	0.3	10	2.67	3.29
12	15	5	0.3	10	3	3.22
13	15	5	0.3	10	3	3.20
14	15	5	0.3	10	3	3.02
15	10	5	0.3	10	2	3.14
16	21	5	0.3	10	4.2	3.18
17	35	7	0.3	10	5	3.05
18	13	5	0.3	20	2.6	6.26
19	12	3	0.5	0	4	1.57

Journal Pre-proof

20	13	3	0.5	0	4.33	1.54
21	28	7	0.5	0	4	1.51
22	37	7	0.5	0	5.29	1.48
23	15	5	0.5	10	3	3.22
24	3	3	0.5	20	1	6.11
25	12	3	0.5	20	4	6.45
26	10	7	0.5	20	1.43	6.39
27	60	7	0.5	20	8.57	6.23

Table 3: BRC25 roller compaction experimental conditions.

Run	N_s (rpm)	N_r (rpm)	SiC (%)	R_f ( )	S ( )
1	56.5	6	0.1	5	1.5
2	62.5	6	0.1	7.5	1.5
3	73.2	6	0.1	11.25	1.5
4	133.0	12	0.1	5	1.5
5	137.0	12	0.1	7.5	1.5
6	141.0	12	0.1	11.25	1.5

3.8. Statistical analysis and goodness-of-fit measures

Design of experiments and subsequent statistical analysis was performed with the Design Expert® 11 statistical software from Stat–Ease Inc. Data visualisation and model fitting was also carried out using R (version 3.6.1) with the integrated development environment RStudio (version 1.1.383).

Fitting of data-driven models was carried out using standard multiple linear regression techniques. Model reduction was performed using analysis of variance (ANOVA) tables. The R-squared value, which explains the proportion of explained variation for linear models, is used to assess goodness-of-fit. Adjusted and predicted R-squared values are used to compare model performance and avoid over-fitting. Further details on the fitting methods applied here can be found in ref. [53].

Journal Pre-proof

The calibration and testing of models outlined in Section 2.3.6 was performed in MATLAB® R2018b (version 9.5.0). The performance of these non-linear models was evaluated using the root mean squared error (RMSE). The root mean squared error can be normalised (NRMSE) to allow for easier comparison of the predictive power of different models. Typically, the RMSE is normalised by the mean value of the measured data or the range of the measured data. The RMSE of the ribbon relative density has normally been scaled using its mean in the literature. However, this leads to the impression of a very low error, as the range over which we would like to predict is typically much smaller than the mean. In this study, both normalisations are reported to allow comparison with existing literature, while also giving a better idea of the fit of the models within the data range.

4. Results and Discussions

4.1. Properties of powders and blends

The particle size distributions of GFN, MCC and blends were measured. The key responses are included in Table 7 in Appendix A. The key flow responses from compressibility and shear testing are reported in Table 4. The addition of silicon dioxide marginally increased the angle of internal friction. As there is limited dependence on SiO_2 level for the three blends considered, an average value $\delta = 32.33^{\circ}$ is chosen for modelling. The wall friction angle was tested on all materials at three roughness values as described in Section 3.3.6. The wall friction angle ϕ_w increases with roughness value for all materials as expected. This is shown in Figure 9. The appropriate value of roughness is difficult to assess, while the preshear stress of $9\,\text{kPa}$ can be considered to be typically less then the wall stresses experienced in the feed region. Thus, the highest roughness value is chosen here. Given the weak variation of wall friction between the formulations in the experimental design, an average value of $\phi_w = 26.09^{\circ}$ is adopted. In the literature, a roughness value if $0.4\,\mu\text{m}$ has been used [13, 55, 1], while Toson et al. [16] prescribed a wall friction angle of 15° across their formulations. Reynolds et al. [13] suggest that, provided the values of δ and ϕ_w are not very low, the predicted ribbon density varies only slowly with these values. The addition of MCC and SiO_2 reduces the cohesion and compressibility percentage C_p of the formulations, while increasing their flow function. Thus,

the blends flow better and should allow for more consistent feeding into the roller compactor.

Table 4: Density and flow properties of powders and blends.

Formulation	δ (°)	ϕ_w (°)	C^* (kPa)	f_c (-)	C_p (%)	CBD ($g\,cm^{-3}$)	ρ_T ($g\,cm^{-3}$)	γ_0 (-)	K (-)
GFN	29.3	23.78	1.09	4.03	47.00	0.33	1.350	0.5616	10.2099
MCC	21.76	28.42	0.97	4.55	17.99	0.36	1.566	0.2820	4.5451
GFN-MCC	29.08	24.50	1.27	3.52	42.88	0.36	1.369	0.4311	6.7182
F_0	28.41	24.43	1.30	3.51	38.30	0.44	1.366	0.4461	7.0065
$F_{0.1}$	32.14	26.29	1.03	4.25	25.17	0.46	1.367	0.4941	8.1630
$F_{0.3}$	31.80	27.40	0.96	4.55	24.86	0.46	1.368	0.4350	6.7888
$F_{0.5}$	33.05	24.59	0.85	5.07	18.31	0.49	1.369	0.4425	6.9663

4.2. Uniaxial compaction

Uniaxial compaction is conducted as described in Section 3.4 for each material and formulation. The values of γ_0 and K fitted from a non-linear regression of the data to equation (9) are listed in Table 4. These values indicate that GFN has a much higher K value than MCC indicating it compresses slowly with increasing pressure. In contrast, MCC has a low reference relative density and compresses much more quickly with increasing pressure. The behaviour of the blends lies in between and the compression behaviour is largely insensitive to the level of SiO_2 The fitted relative density-pressure profiles are shown in Figure 3. The uniaxial compaction tests provide initial guesses for the compression parameters in the nip region and show the general compression behaviour of the blends.

Figure 3: Uniaxial compaction compressibility profiles. MCC (bottom line) and GFN (top line) show a clearly different behaviour while the formulation density-pressure profiles are very similar as suggested by their fitted values of γ_0 and K in table 4

4.3. Statistical analysis of DoE

The experimental DoE for the FMRC has been described in Section 3.7. The key responses are listed in Table 5. These responses from the BRC25 experiments are also listed. Ribbon density and thickness are measured in triplicates as outlined in Section 3. The throughput is calculated from equation (2) using the average values for ribbon density and thickness (roll gap). The values of c_s for each run are calculated using equation (3), again using average values for γ_r and S. Before applying the mass throughput and Johanson models, it is useful to do a statistical analysis to consider the significant input factors driving the variation in the responses in Table 5. We fit the response behaviour using multiple linear regression and reduce the resulting models to their significant factors. Due to a high degree of co-linearity between the roll speed and screw speed, the ratio of screw speed to roll speed is used as a factor. The other two factors used are roll force and SiO_2 level. Interestingly, the SiO_2 level does not have a statistically significant influence on any of the responses considered. This further supports the use of average values for the angle of internal friction and angle of wall friction. Nevertheless a minimum amount of SiO_2 is needed, as the formulation does not feed consistently in its absence. This is captured by the high C_p values of the formulation without SiO_2 reported in Section 4.1, indicating poor flow behaviour from a low stress state.

Roll force is the only factor to have a statistically significant effect on ribbon density with 74% of the observed variability explained by a quadratic function of roll force. This accounts for a reduction in the compression rate at higher roll forces as the compact porosity decreases.

Ribbon thickness can be described well using a quadratic function of screw speed to roll speed ratio. This function accounts for over 92% of the observed variation in the ribbon thickness. Roll force does not appear as a significant factor in the model, once screw speed to roll speed ratio and its square are included. Despite this, there is a strong negative correlation between roll force and thickness. This is captured in the limits of screw speed to roll speed ratio (and hence thickness) that are possible at each roll force. For example, at higher roll forces, screw speed to roll speed ratios as low as 1 are possible, thus allowing very thin ribbons to be manufactured. At the lowest roll force the minimum ratio is 4. Below this no intact ribbons are made. Thus ribbons are thicker in general for lower roll forces. Within the range of possible values of N_s / N_r, the ribbon thickness is observed to depend on this ratio.

Journal Pre-proof

The value of the screw function c_s corresponds to the mass conveyed per screw revolution in each run and is calculated by dividing the throughput by the screw speed. The value of c_s is observed to depend only the value of N_s / N_r. The explained variation of over 93%, with similar values of the adjusted and predicted R-squared values, suggests that the functional relationship described in equation (4) is likely to be useful for prediction.

Table 5: Key responses from DoE on the FMRC and on the BRC25. Run 3 on the BRC25 was excluded as the variation in ribbon thickness indicated the process had not reached stable control. Runs 1 and 2 on the BRC25 are used to calibrate the screw function indicated by 'F' but only used for prediction of ribbon density, indicated by 'P'.

	Roller compaction FMRC					
Run	Ribbon density ($g\,cm^{-3}$)	γ_r (-)	S (nm)	$\dot{m}$ ($kg\,h^{-1}$)	c_s (g)	Fitting or Prediction (F/P)
1	0.9813	0.7180	2.12	2.94	3.98	F
2	1.0001	0.7317	2.69	3.80	4.99	F
3	0.9901	0.7244	2.51	8.20	4.88	P
4	1.0429	0.7631	2.69	9.25	4.13	P
5	1.0357	0.7578	2.21	5.38	6.10	P
6	1.0807	0.7907	0.86	1.31	7.56	F
7	1.0849	0.7938	2.05	3.14	5.94	F
8	1.1190	0.8187	1.15	4.23	7.14	P
9	1.088	0.7961	1.88	6.73	1.94	P
10	1.0007	0.7316	2.63	6.19	4.59	P
11	1.1403	0.8337	1.85	2.98	5.84	F
12	1.0442	0.7634	2.02	4.97	5.54	P
13	1.0308	0.7536	2.20	5.33	6.04	P
14	1.0491	0.7670	2.21	5.46	6.07	P
15	1.0798	0.7894	1.63	4.13	6.90	P

Journal Pre-proof

16	1.0723	0.7839	2.66	6.71	5.29	P
17	1.0694	0.7818	2.00	7.04	3.41	P
18	1.1653	0.8519	1.81	4.96	6.23	P
19	0.9618	0.7026	2.46	3.34	4.72	F
20	0.9941	0.7262	2.61	3.66	4.60	F
21	0.9876	0.7214	2.39	7.79	4.62	P
22	1.0104	0.7381	2.66	8.85	4.04	P
23	1.0466	0.7645	2.04	5.02	5.64	P
24	1.0983	0.8023	0.74	1.14	6.88	F
25	1.0817	0.7902	2.41	3.69	5.22	F
26	1.1229	0.8203	1.10	4.08	6.87	P
27	1.1085	0.8098	1.82	6.64	1.92	P
	Roller compactor: BRC25					
1	1.0826	0.7900	1.52	11.63	3.43	F/P
2	1.0534	0.7686	1.61	11.99	3.20	F/P
4	1.0682	0.7794	1.54	23.26	2.91	P
5	1.1251	0.8210	1.46	23.22	2.83	P
6	1.1330	0.8267	1.51	24.19	2.86	P

4.4. Limitations of screw constant and calibration of screw function

It is clear from statistical analysis of the data that the common assumption of a screw constant c_s, which is independent of the process parameters, is not suitable for this particular blend and equipment. This can be seen by fitting a constant c_s and comparing the measured and predicted values of S and the throughput. Figure 4 plots the throughput for each run coloured by roll speed. Applying the algorithm in Section 2.3.6 we fit c_s using the low-throughput (LT) data ($N_r = 3$). The runs used for model calibration are indicated by the letter 'F' in Table 5, while the ones used for prediction are indicated by the letter 'P'. A value $c_s = 4.929\,\mathrm{g}$ is obtained by fitting the LT data. It should be highlighted that prediction of S and throughput for the high-throughput (HT) data requires the calculation of the ribbon density for the HT data, which in practice will not

Journal Pre-proof

be known. Thus, γ_0 and K must be calculated using the algorithm in Figure 2 before prediction on HT data is possible. In order to ensure that any lack of fit of S for the HT data was not due to poor ribbon density prediction it was confirmed that values predicted for S using the measured ribbon densities and fitted c_s gave a similar lack of fit. The predicted values of S and throughput are compared with the measured values for both LT and HT data in Figures 5a and 5b. For lower ribbon thicknesses, the prediction underestimates the true value, while the thickness is overestimated dramatically for some larger values. Similarly, the throughput is underestimated at low values and produces large overestimations for some high values. This is unsurprising, as a single value of c_s cannot reproduce the range of values of c_s from $1.92\,\mathrm{g}$ to $7.56\,\mathrm{g}$ for individual runs. However, the statistical analysis suggests that a simple predictive model can be implemented. Thus, fitting the LT data to equation (4) we find $c_{s0} = 7.988\,\mathrm{g}$ and $c_{s1} = -0.788\,\mathrm{g}$. The model prediction for c_s as a function of N_s / N_r is shown in Figure 6. Using this function, we see that the predicted vs. actual plots for S (Figure 7a) and throughput (Figure 7b) show much better agreement and the residuals are distributed around the line of perfect fit. The RMSE for the model calibration and validation of ribbon thickness and throughput, for both constant and linear expressions for c_s, are shown in Table 6. It is clear that the use of a linear expression of c_s decreases the error significantly, particularly for prediction on the validation data.

As the BRC25 has a different screw configuration, the results from the FMRC cannot be transferred to this equipment. Application of a gap controlled model would address this issue provided the model of ribbon density was transferable and equation (2) could be applied to predict throughput. However, in the absence of data on the in-process roll gap it is necessary to calibrate a new model for the screw function based on process data. Run 3 on the BRC25 was discarded from the sample due to large variations in the thickness of analysed ribbons indicating that process equilibrium was not achieved. Both constant and linear models for c_s were fitted to the LT data (runs 1 and 2). It was found that the c_s decreased linearly with N_s / N_r and applying this relationship led to a substantial decrease in the RMSE for both ribbon thickness and throughput (see Table 6). Despite only being fitted on the two available LT experiments for the BRC25, the predicted c_s values matched well for the HT data, further validating the screw function in equation (4). The fitted values were $c_{s0} = 5.638\,\mathrm{g}$ and $c_{s1} = -0.234\,\mathrm{g}$.

Figure 4: Throughput from different experiments. Models are calibrated using low throughput data ($N_r = 3$).

Figure 5: Prediction of (a) ribbon thickness vs. actual ribbon thickness and (b) throughput vs. actual throughput using a screw constant c_s.

Figure 6: Fit of c_s with $\frac{N_s}{N_r}$.

Figure 7: (a) Predicted ribbon thickness vs. actual ribbon thickness and (b) predicted throughput vs. actual throughput using the screw function in equation (4).

Table 4: Root mean square error from the different models. The root mean square error is reported for model calibration on the FMRC, model validation on the FMRC and prediction on the BRC25. The RMSE is also reported as a percentage of the mean value and total range of each variable across all experiments for ribbon density. The RMSE is reported as a percentage of the mean value and total range of each variable within each roller compactor for ribbon thickness and throughput. The narrow range of thicknesses in the BRC25 leads to apparently large RMSE errors normalised by thickness range.

	S		Throughput		γ_r	
	constant c_s	linear c_s	constant c_s	linear c_s	constant c_s	linear c_s
FMRC calibration						
RMSE	0.27	0.19	0.39	0.26	0.0128	0.0119
RMSE% mean	12.93	9.00	7.69	5.15	1.66	1.54
RMSE% range	13.92	9.69	4.93	3.30	10.42	9.66

Journal Pre-proof

FMRC						
validation						
RMSE	1.15	0.26	3.87	0.94	0.0194	0.0153
RMSE% mean	60.08	12.71	75.94	18.38	2.50	1.98
RMSE% range	55.82	13.68	48.70	11.79	15.73	12.40
BRC25						
RMSE	0.181	0.044	2.81	0.68	0.0268	0.0221
RMSE% mean	11.84	2.88	14.88	3.63	3.48	2.86
RMSE% range	120.64	29.32	22.35	5.45	21.81	17.97

4.5. Training and validation of model on FMRC DoE

The main challenge of this work was to implement a model for scale-up of a roller compaction process for a very high drug loading of a difficult to process API. This was achieved using the algorithm described in Section 2.3.6 and presented in Figure 2. Applying this algorithm on the LT data gives values of $\gamma_0 = 0.590$ and $K = 15.613$ where a linear screw function has been used. The comparison between the model prediction and measured ribbon density values are shown in Figure 8a. The fitted relationship between the ribbon density and the maximum pressure attained between the rolls is shown in Figure 8b. The plot includes the 95% confidence bands on the model fit. The experimental data is also shown, with the values of P_{max} predicted using equation (13). Applying a constant screw function gives $\gamma_0 = 0.597$ and $K = 16.894$. The choice of mass flow description in the screw has less of an impact on the ribbon density prediction compared to ribbon thickness and throughput, as small changes in the prediction of S do not have a large impact on the predicted density. However, applying the screw function does give a slight reduction in the RMSE reported in Table 6. The RMSE increased slightly on the validation data at higher throughputs but not substantially. Fitting the model to all the data (LT and HT) results in values $\gamma_0 = 0.596$ and $K = 15.668$ indicating the overall variation is already captured by fitting on the LT data. We note that the RMSE normalised by the mean indicates a similar magnitude of error ($< 2\%$) as achieved in refs. [13, 16]. The RMSE normalised by the data range ($\approx 10\%$) indicates that the model can capture the general behaviour of the ribbon density in response to the process parameters, but very high accuracy predictions are not possible.

Journal Pre-proof

Comparing the fitted values of K with those found in uniaxial compaction experiments shows that the values fitted from actual roller compaction experiments are approximately twice those found in the uniaxial experiments. Thus, the uniaxial experiments are useful for comparison of compressibility between pure materials and blends but should only be used to provide initial guesses for the values of γ_0 and K for the roller compactor.

Figure 8: (a) Predicted ribbon density vs. actual ribbon density (b) Fit of ribbon density vs. calculated maximum pressure.

4.6. Prediction of ribbon density on BRC25 RC

Scale-up within a roller compactor is very important for efficient process design. Often a process also has to be transferred between different roller compactors. In this work, we consider the suitability of the presented model to transfer the process from the FMRC to the BRC25. The key difference between the two roller compactors in terms of compaction is the larger rolls on the BRC25 ($250\,\text{mm}$ vs. $100\,\text{mm}$). When true gap control is used it is unnecessary to find the throughput behaviour by fitting a screw function c_s. However, as indicated above, the in-process roll gap has not been measured in this work so it is necessary to calibrate a model to predict the roll gap for each experiment in the ribbon density model based on the screw speed and roll speed. This has been done in Section 4.4. The ribbon density model can now be used to predict the ribbon density on the BRC25 using the previously fitted values γ_0 and K. The RMSE values of the resulting predictions are shown in Table 6. The prediction RMSE has risen to nearly 18% of the ribbon density range. The individual data points are shown in Figures 8a and 8b.

4.7. Discussion

The models developed in this work show that the commonly used screw constant was insufficient for prediction of mass throughput and ribbon thickness for a high drug load formulation with poor flow properties during development on the FMRC. A screw function which depends linearly on the ratio of screw speed to roll speed had a much improved fit with the experimental data. The BRC25 showed the same linear decrease in the mass conveyed per

revolution with N_s / N_r. The gradient of the decrease was less than in the FMRC, which is unsurprising as the BRC25 is equipped with a much more sophisticated feeding system consisting of a feeding and tamping screw. This new screw function has been incorporated into an algorithm based on the models of Johanson [20] and Reynolds [13]. The model can be fitted on low-throughput data and, provided that this data covers the relevant ranges of N_s / N_r and γ_r, it has been shown that it can predict the ribbon thickness, throughput and ribbon density for high-throughput experiments with a reasonable degree of accuracy. Thus, this model can be used for targeting specific ribbon densities at a higher throughputs and identifying the operating space to hit these targets.

The application of the model for transfer of process knowledge between roller compactors is desirable. However care should be taken here. The use of the model trained on the FMRC to predict the ribbon density on the BRC25 shows a decreased accuracy. This should be expected as the material law applied in the nip region is overly simplistic. Rather then just containing information about the formulation in question the values γ_0 and K can be considered to be lumped parameters, containing information about the formulation compression behaviour and the equipment in question. This is also evident from the comparison between the parameter values for uniaxial compaction and roller compaction on the FMRC. Thus, while the model gives some estimates for the transfer between roller compactors, it should only be used for rough estimation to guide experiments on the new RC. The method of model development based on low-throughput data can be expected to be valid across different roller compactors, provided the range of ribbon densities and screw speed to roll speed ratios needed for prediction are covered in calibration data on that roller compactor. The range of material throughputs in this study is $1.3\,\mathrm{kg\,h^{-1}}$ to $24.2\,\mathrm{kg\,h^{-1}}$ due to limitations on material supply and RC equipment. The next step is to assess the accuracy of the approach for scale-up by roll speed, roll width and roll diameter on RC equipment which is capable of manufacturing scale throughputs ($\gtrsim 100\,\mathrm{kg\,h^{-1}}$), for both low and high drug load formulations.

5. Conclusions

This work presents a model based development of a roller compression process for an API at high drug loading. A new description for the mass flow rate in the screw feeder has been

incorporated to account for a reduced feeding performance at higher screw speed to roll speed ratios. The model is calibrated based on low-throughput data at a low roll speed and used to predict ribbon thickness and throughputs at higher roll speeds. It is shown that the resulting prediction is much more accurate than that arrived at using a mass flow rate which only depends linearly on the screw speed. The compression behaviour in the nip region is characterised by a commonly used constitutive material law based on a pre-consolidation density γ_0 and compressibility factor K. The values of K depends on the configuration of the equipment used for compression. Thus, uniaxial compaction experiments tend to strongly over-predict actual roller compactor ribbon densities and generally models fitted on one roller compactor will produce poor predictions on a different roller compactor. This is shown here for prediction of ribbon density on the BRC25, based on models developed on the FMRC.

It has been demonstrated that scale-up is possible on an individual roller compactor from low-throughput experiments. The model is developed by an iterative fitting procedure applying linear and non-linear regression techniques on low throughput data. This gives fitted relationships between the ribbon thickness, throughput and ribbon density and the screw speed, screw speed to roll speed ratio and the applied roll force. It is shown that these models provide good predictions of these variables at high-throughput, thus providing a useful tool for process scale-up, while maintaining target critical quality attributes.

Acknowledgements

This publication has emanated from research supported in part by a research grant from Science Foundation Ireland (SFI) 'Modelling of Multi-Phase Transport Processes to Enable Automation in Manufacturing, (MOMEnTUM)' and is co-funded under the European Regional Development Fund under Grant Number 14/SP/2750, in partnership with Janssen Pharmaceuticals.

Appendix A. Supplementary data

The particle size distribution parameters d_{10}, d_{50}, d_{90}, along with the mean diameter by volume MV and the specific surface area SSA for each material and formulation are given in Table 7.

Table 7: Particle size information on powders and blends.

Formulation	d_{10} (μm)	d_{50} (μm)	d_{90} (μm)	MV (μm)	SSA (μm)
GFN	4.68	19.01	88.58	37.67	0.54
MCC	19.67	118.00	238.07	124.27	0.12
GFN-MCC	5.60	24.65	172.17	64.63	0.45
F_0	5.09	23.00	158.37	58.79	0.48
$F_{0.1}$	5.08	23.17	149.73	57.47	0.48
$F_{0.3}$	5.19	23.45	139.07	52.82	0.48
$F_{0.5}$	5.26	22.19	130.00	49.17	0.48

The dependence of the angle of wall friction ϕ on the wall roughness is shown in Figure 9.

Figure 9: Dependence of wall friction angle on material roughness for different formulations.

References

[1] A. P. Gago, G. Reynolds, P. Kleinebudde, Impact of roll compactor scale on ribbon density, Powder Technology 337 (2018) 92–103.

[2] H. L. Reimer, P. Kleinebudde, Hybrid modeling of roll compaction processes with the styl'one evolution, Powder technology 341 (2019) 66–74.

[3] G. E. Peck, J. L. Soh, K. R. Morris, Dry granulation, in: Pharmaceutical Dosage Forms-Tablets, CRC Press, 2008, pp. 319–352.

[4] P. Kleinebudde, Roll compaction/dry granulation: pharmaceutical applications, European Journal of Pharmaceutics and biopharmaceutics 58 (2) (2004) 317–326.

[5] A. Rogers, A. Hashemi, M. Ierapetritou, Modeling of particulate processes for the continuous manufacture of solid-based pharmaceutical dosage forms, Processes 1 (2) (2013) 67–127.

[6] S. Yu, B. Gururajan, G. Reynolds, R. Roberts, M. J. Adams, C.-Y. Wu, A comparative study of roll compaction of free-flowing and cohesive pharmaceutical powders, International journal of pharmaceutics 428 (1-2) (2012) 39–47.

[7] M. G. Herting, P. Kleinebudde, Studies on the reduction of tensile strength of tablets after roll compaction/dry granulation, European Journal of Pharmaceutics and Biopharmaceutics 70 (1) (2008) 372–379.

[8] C. C. Sun, P. Kleinebudde, Mini review: Mechanisms to the loss of tabletability by dry granulation, European Journal of Pharmaceutics and Biopharmaceutics 106 (2016) 9–14.

[9] Y. Teng, Z. Qiu, H. Wen, Systematical approach of formulation and process development using roller compaction, European journal of pharmaceutics and biopharmaceutics 73 (2) (2009) 219–229.

[10] M. Leane, K. Pitt, G. Reynolds, M. C. S. M. W. Group, A proposal for a drug product manufacturing classification system (mcs) for oral solid dosage forms, Pharmaceutical development and technology 20 (1) (2015) 12–21.

[11] M. Leane, K. Pitt, G. K. Reynolds, N. Dawson, I. Ziegler, A. Szepes, A. M. Crean, R. Dall Agnol, M. C. S. M. W. Group, et al., Manufacturing classification system in the real world: factors influencing manufacturing process choices for filed commercial oral solid dosage formulations, case studies from industry and considerations for continuous processing, Pharmaceutical development and technology 23 (10) (2018) 964–977.

[12] A. L. P. Queiroz, W. Faisal, K. Devine, H. Garvie-Cook, S. Vucen, A. M. Crean, The application of percolation threshold theory to predict compaction behaviour of pharmaceutical powder blends, Powder Technology 354 (2019) 188–198.

[13] G. Reynolds, R. Ingale, R. Roberts, S. Kothari, B. Gururajan, Practical application of roller compaction process modeling, Computers & chemical engineering 34 (7) (2010) 1049–1057.

[14] B. C. Hancock, J. T. Colvin, M. P. Mullarney, A. V. Zinchuk, Pharmaceutical powders, blends, dry granulations, and immediate-release tablets, Pharmaceutical technology 6480.

[15] A. V. Zinchuk, M. P. Mullarney, B. C. Hancock, Simulation of roller compaction using a laboratory scale compaction simulator, International journal of pharmaceutics 269 (2) (2004) 403–415.

[16] P. Toson, D. G. Lopes, R. Paus, A. Kumar, J. Geens, S. Stibale, J. Quodbach, P.

Kleinebudde, W.-K. Hsiao, J. Khinast, Model-based approach to the design of pharmaceutical roller-compaction processes, International Journal of Pharmaceutics: X 1 (2019) 100005.

[17] A. Rogers, M. Ierapetritou, Challenges and opportunities in modeling pharmaceutical manufacturing processes, Computers & Chemical Engineering 81 (2015) 32–39.

[18] A. Michrafy, A. Zavaliangos, J. Cunningham, 4 - dry granulation process modeling, in: P. Pandey, R. Bharadwaj (Eds.), Predictive Modeling of Pharmaceutical Unit Operations, Woodhead Publishing, 2017, pp. 71 – 97. doi:https://doi.org/10.1016/B978-0-08-100154-7.00004-1.
URL
http://www.sciencedirect.com/science/article/pii/B9780081001547000041

[19] N. Souihi, G. Reynolds, P. Tajarobi, H. Wikström, G. Haeffler, M. Josefson, J. Trygg, Roll compaction process modeling: transfer between equipment and impact of process parameters, International journal of pharmaceutics 484 (1-2) (2015) 192–206.

[20] J. Johanson, A rolling theory for granular solids, ASME, 1965.

[21] G. Bindhumadhavan, J. Seville, M. Adams, R. Greenwood, S. Fitzpatrick, Roll compaction of a pharmaceutical excipient: Experimental validation of rolling theory for granular solids, Chemical Engineering Science 60 (14) (2005) 3891–3897.

[22] J. M. Rowe, J. R. Crison, T. J. Carragher, N. Vatsaraj, R. J. Mccann, F. Nikfar, Mechanistic insights into the scale-up of the roller compaction process: A practical and dimensionless approach, Journal of pharmaceutical sciences 102 (10) (2013) 3586–3595.

[23] M. Bi, F. Alvarez-Nunez, F. Alvarez, Evaluating and modifying johanson's rolling model to improve its predictability, Journal of pharmaceutical sciences 103 (7) (2014) 2062–2071.

[24] E. Gavi, G. K. Reynolds, System model of a tablet manufacturing process, Computers & Chemical Engineering 71 (2014) 130–140.

[25] P. Guigon, O. Simon, Roll press designâ€"influence of force feed systems on compaction, Powder Technology 130 (1) (2003) 41 – 48. doi:https://doi.org/10.1016/S0032-5910(02)00223-1.
URL

http://www.sciencedirect.com/science/article/pii/S0032591002002231

[26] L. L. Augsburger, S. W. Hoag, Pharmaceutical dosage forms-tablets, CRC press, 2016.

[27] D. M. Parikh, Handbook of pharmaceutical granulation technology, CRC Press, 2016.

[28] P. Guigon, O. Simon, K. Saleh, G. Bindhumadhavan, M. J. Adams, J. P. Seville, Roll pressing, in: Handbook of Powder Technology, Vol. 11, Elsevier, 2007, pp. 255–288.

[29] J. C. Cunningham, A. Zavaliangos, Experimental studies and modeling of the roller compaction of pharmaceutical powders, Drexel University, 2005.

[30] J. C. Cunningham, D. Winstead, A. Zavaliangos, Understanding variation in roller compaction through finite element-based process modeling, Computers & chemical engineering 34 (7) (2010) 1058–1071.

[31] R. T. Dec, A. Zavaliangos, J. C. Cunningham, Comparison of various modeling methods for analysis of powder compaction in roller press, Powder Technology 130 (1-3) (2003) 265–271.

[32] V. Katashinskii, Analytical determination of specific pressure during the rolling of metal powders, Soviet Powder Metallurgy and Metal Ceramics 5 (10) (1966) 765–772.

[33] M. Balicki, et al., Numerical methods for predicting roll press powder compaction parameters, École des Mines D'Albi-Carmaux, France.

[34] A. Michrafy, H. Diarra, J. A. Dodds, M. Michrafy, Experimental and numerical analyses of homogeneity over strip width in roll compaction, Powder technology 206 (1-2) (2011) 154–160.

[35] A. Michrafy, H. Diarra, J. A. Dodds, M. Michrafy, L. Penazzi, Analysis of strain stress state in roller compaction process, Powder technology 208 (2) (2011) 417–422.

[36] A. R. Muliadi, J. D. Litster, C. R. Wassgren, Modeling the powder roll compaction process: Comparison of 2-d finite element method and the rolling theory for granular solids (johanson's model), Powder technology 221 (2012) 90–100.

[37] A. R. Muliadi, J. D. Litster, C. R. Wassgren, Validation of 3-d finite element analysis for predicting the density distribution of roll compacted pharmaceutical powder, Powder technology 237 (2013) 386–399.

[38] Y. Liu, C. Wassgren, Modifications to johanson's roll compaction model for improved relative density predictions, Powder technology 297 (2016) 294–302.

[39] A. Mazor, L. Orefice, A. Michrafy, A. De Ryck, J. G. Khinast, A combined dem & fem approach for modelling roll compaction process, Powder Technology 337 (2018) 3–16.

[40] A. Krok, C.-Y. Wu, Evolutions of temperature and density during roll compaction of a pharmaceutical excipient, International Journal of Pharmaceutics 572 (2019) 118822. doi:https://doi.org/10.1016/j.ijpharm.2019.118822.
URL http://www.sciencedirect.com/science/article/pii/S0378517319308671

[41] T. Sinha, J. S. Curtis, B. C. Hancock, C. Wassgren, A study on the sensitivity of drucker–prager cap model parameters during the decompression phase of powder compaction simulations, Powder Technology 198 (2) (2010) 315–324.

[42] A. Roberts, The influence of granular vortex motion on the volumetric performance of enclosed screw conveyors, Powder Technology 103 (1) (1999) 56–67.

[43] S.-H. Hsu, G. V. Reklaitis, V. Venkatasubramanian, Modeling and control of roller compaction for pharmaceutical manufacturing. part i: Process dynamics and control framework, Journal of Pharmaceutical Innovation 5 (1-2) (2010) 14–23.

[44] S.-H. Hsu, G. V. Reklaitis, V. Venkatasubramania, Modeling and control of roller compaction for pharmaceutical manufacturing, Journal of Pharmaceutical Innovation 5 (1-2) (2010) 24–36.

[45] F. Boukouvala, V. Niotis, R. Ramachandran, F. J. Muzzio, M. G. Ierapetritou, An integrated approach for dynamic flowsheet modeling and sensitivity analysis of a continuous tablet manufacturing process, Computers & Chemical Engineering 42 (2012) 30–47.

[46] R. M. Nedderman, Statics and kinematics of granular materials, Cambridge University Press, 2005.

[47] J. R. Johanson, Stress and velocity fields in the gravity flow of bulk solids, Journal of applied Mechanics 31 (3) (1964) 499–506.

[48] G. Seber, C. Wild, Nonlinear Regression, Wiley Series in Probability and Statistics, Wiley, 2003.
URL https://books.google.com.pr/books?id=NaU9Sx1VMIMC

[49] K. Sommer, G. Hauser, Flow and compression properties of feed solids for roll-type

Journal Pre-proof

presses and extrusion presses, Powder Technology 130 (1-3) (2003) 272–276.

[50] E. Marshall, A theory for the compaction of incompressible granular materials by rolling, IMA Journal of Applied Mathematics 12 (1) (1973) 21–36.

[51] E. Marshall, The compaction of granular materials by rolling ii. the effect of material compressibility, IMA Journal of Applied Mathematics 13 (3) (1974) 279–298.

[52] S. Lakio, B. Vajna, I. Farkas, H. Salokangas, G. Marosi, J. Yliruusi, Challenges in detecting magnesium stearate distribution in tablets, AAPS PharmSciTech 14 (1) (2013) 435–444.

[53] B. E. Schaller, K. M. Moroney, B. Castro-Dominguez, F. Cronin, J. Belen-Girona, P. Ruane, D. M. Croker, G. M. Walker, Systematic development of a high dosage formulation to enable direct compression of a poorly flowing api: A case study, International Journal of Pharmaceutics doi:https://doi.org/10.1016/j.ijpharm.2019.05.073.
URL
http://www.sciencedirect.com/science/article/pii/S0378517319304387

[54] Y. Wang, T. Li, F. J. Muzzio, B. J. Glasser, Predicting feeder performance based on material flow properties, Powder Technology 308 (2017) 135 – 148. doi:https://doi.org/10.1016/j.powtec.2016.12.010.
URL
http://www.sciencedirect.com/science/article/pii/S0032591016308804

[55] N. Souihi, M. Josefson, P. Tajarobi, B. Gururajan, J. Trygg, Design space estimation of the roller compaction process, Industrial & Engineering Chemistry Research 52 (35) (2013) 12408–12419.

Journal Pre-proof

Journal Pre-proof

Credit Author Statement:

Kevin M. Moroney, Conceptualisation, Methodology, Validation, Data Curation, Software, Formal Analysis, Writing - Original Draft, **Patrick Cronin**, Conceptualisation, Methodology, Investigation, Validation, Writing - Review & Editing **Opeyemi A. Adeleye**, Investigation, Validation, **Barbara E. Schaller**, Conceptualisation, Methodology, Investigation, Validation, Writing - Review & Editing, **Matthew A. Howard**, Conceptualisation, Resources, Writing - Review & Editing , **Bernardo Castro-Dominguez**, Conceptualisation, Methodology, Validation, Investigation, Writing - Review & Editing, **Rohit Ramachandran**, Resources, Writing - Review & Editing, **Gavin M. Walker**, Conceptualisation, Funding Acquisition, Resources, Supervision

Journal Pre-proof

Declaration of interests

☒ The authors declare that they have no known competing financial interests or personal relationships that could have appeared to influence the work reported in this paper.

☐The authors declare the following financial interests/personal relationships which may be considered as potential competing interests:

Journal Pre-proof

Journal Pre-proof

- Model based process development for roller compaction for high dose API (90%)
- New mass transport description for feed screw based on screw speed and roll speed
- Successful process scale-up using model calibrated only on low-throughput data
- Model transfer to different equipment is challenging

Journal Pre-proof

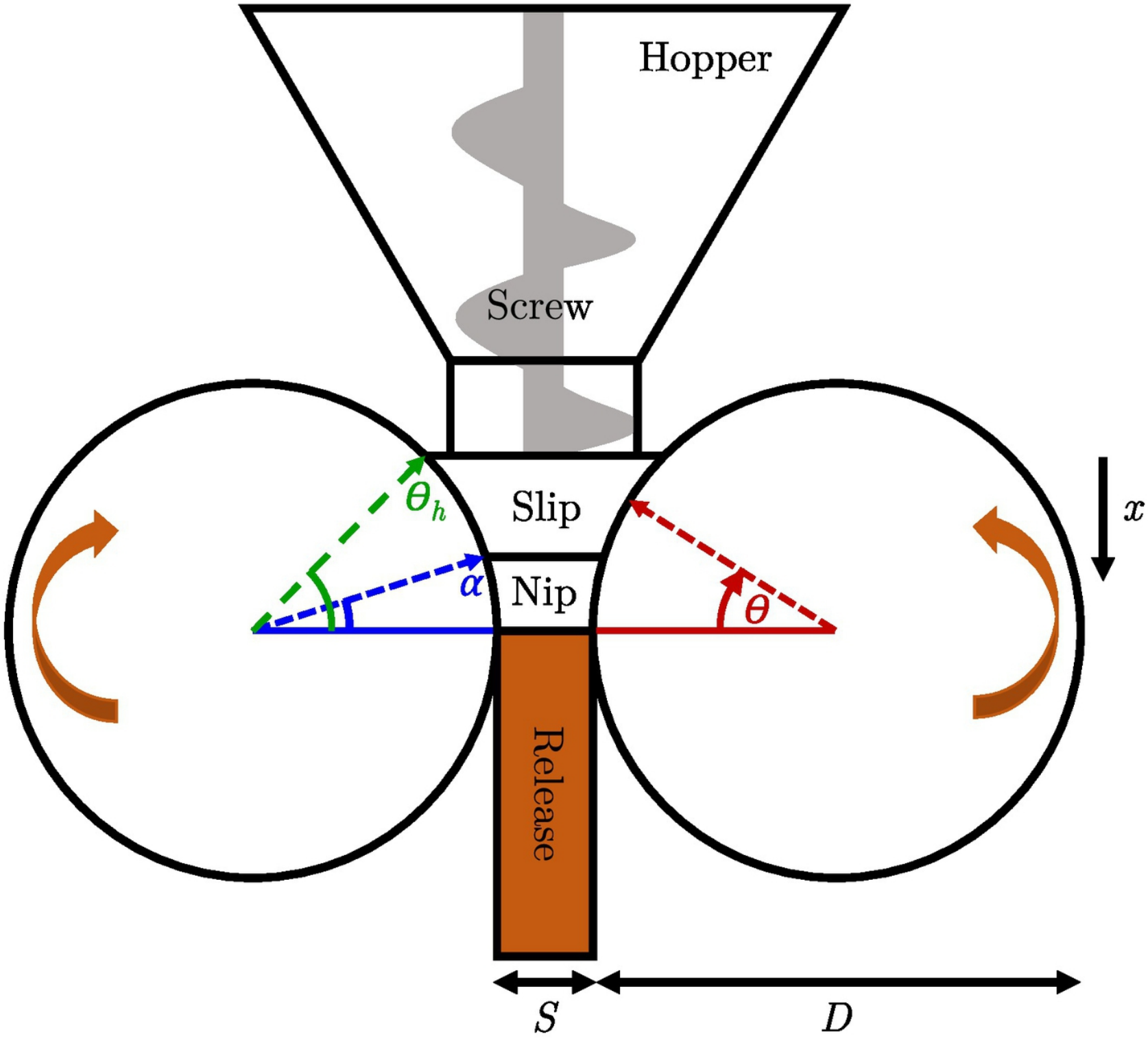

Figure 1

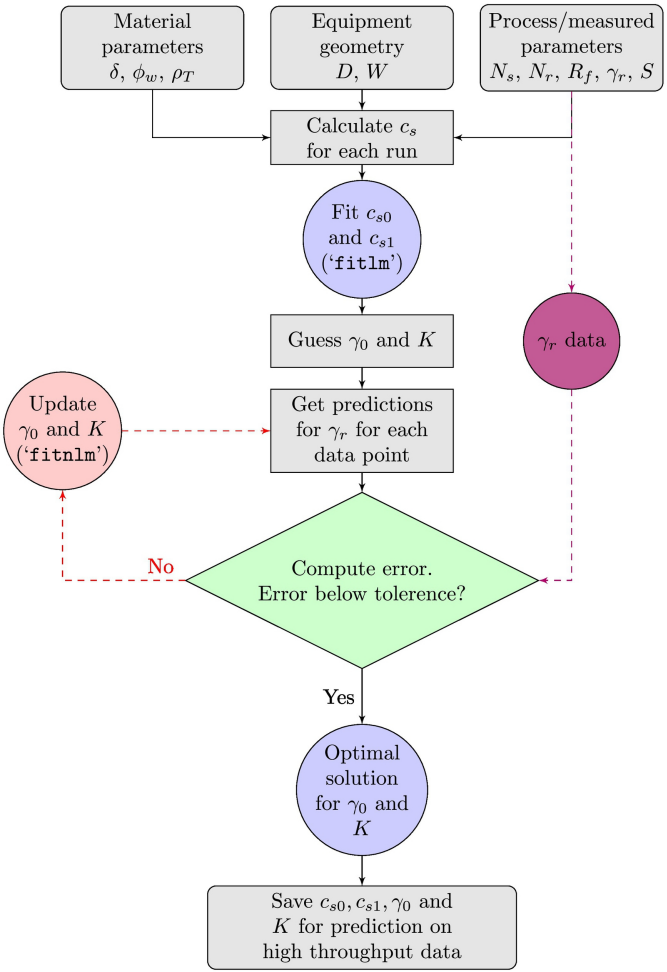
Material parameters δ, ϕ_w, ρ_T
Equipment geometry D, W
Process/measured parameters N_s, N_r, R_f, γ_r, S
Calculate c_s for each run
Fit c_{s0} and c_{s1} ('fitlm')
Guess γ_0 and K
γ_r data
Update γ_0 and K ('fitnlm')
Get predictions for γ_r for each data point
No
Compute error. Error below tolerence?
Yes
Optimal solution for γ_0 and K
Save c_{s0}, c_{s1}, γ_0 and K for prediction on high throughput data

Figure 2

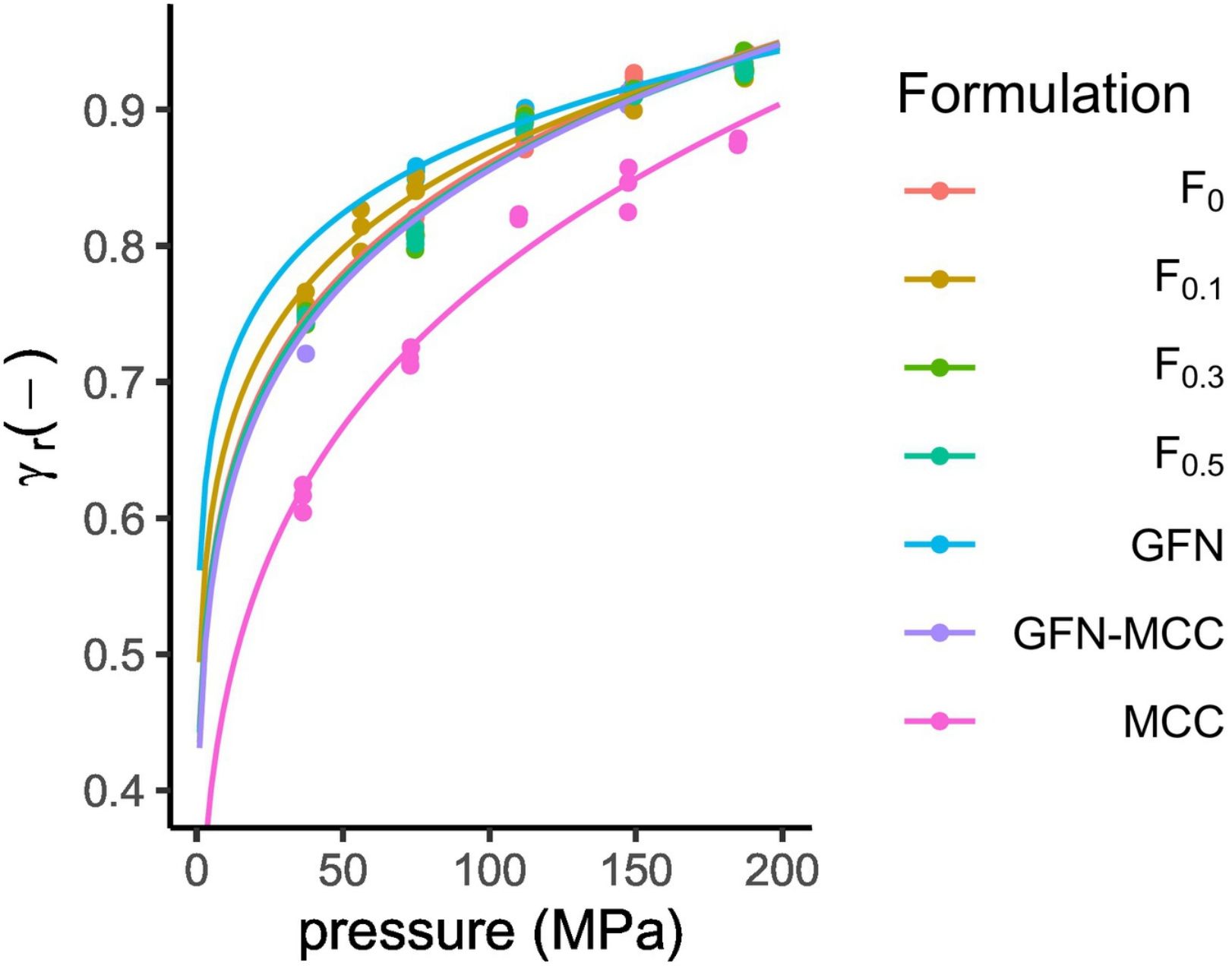
0.9
0.8
0.7
0.6
0.5
0.4
γ r(−)
0
50
100
150
200
pressure (MPa)
Formulation
F0
F0.1
F0.3
F0.5
GFN
GFN-MCC
MCC

Figure 3

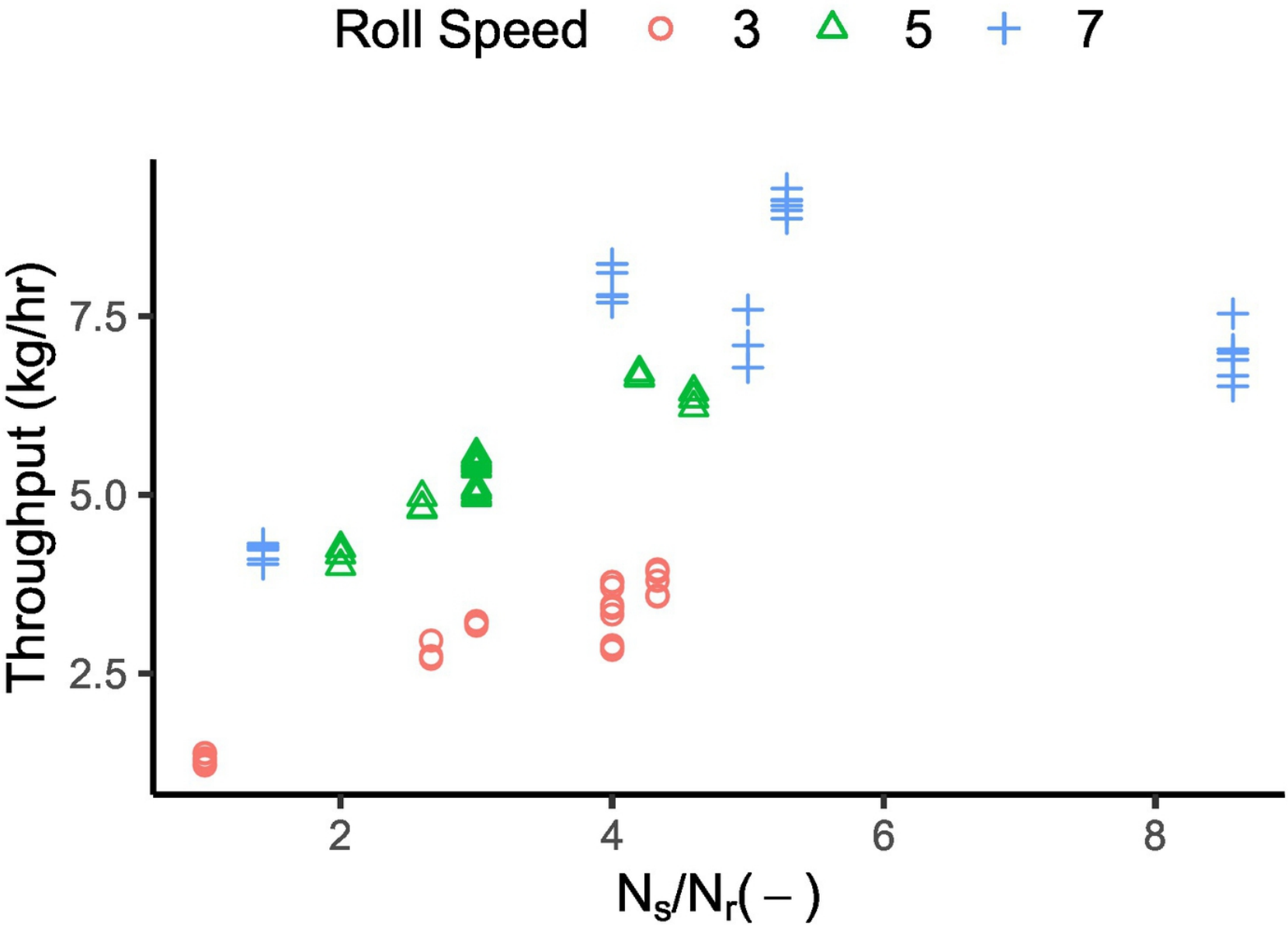

Figure 4

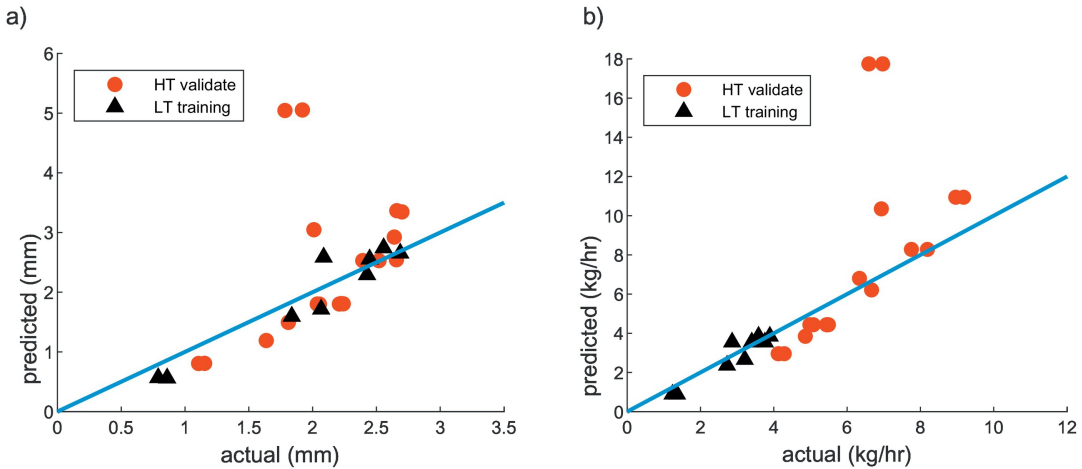
a)
HT validate
LT training
predicted (mm)
actual (mm)
0
0.5
1
1.5
2
2.5
3
3.5
1
2
3
4
5
6
b)
HT validate
LT training
predicted (kg/hr)
actual (kg/hr)
0
2
4
6
8
10
12
2
4
6
8
10
12
14
16
18

Figure 5

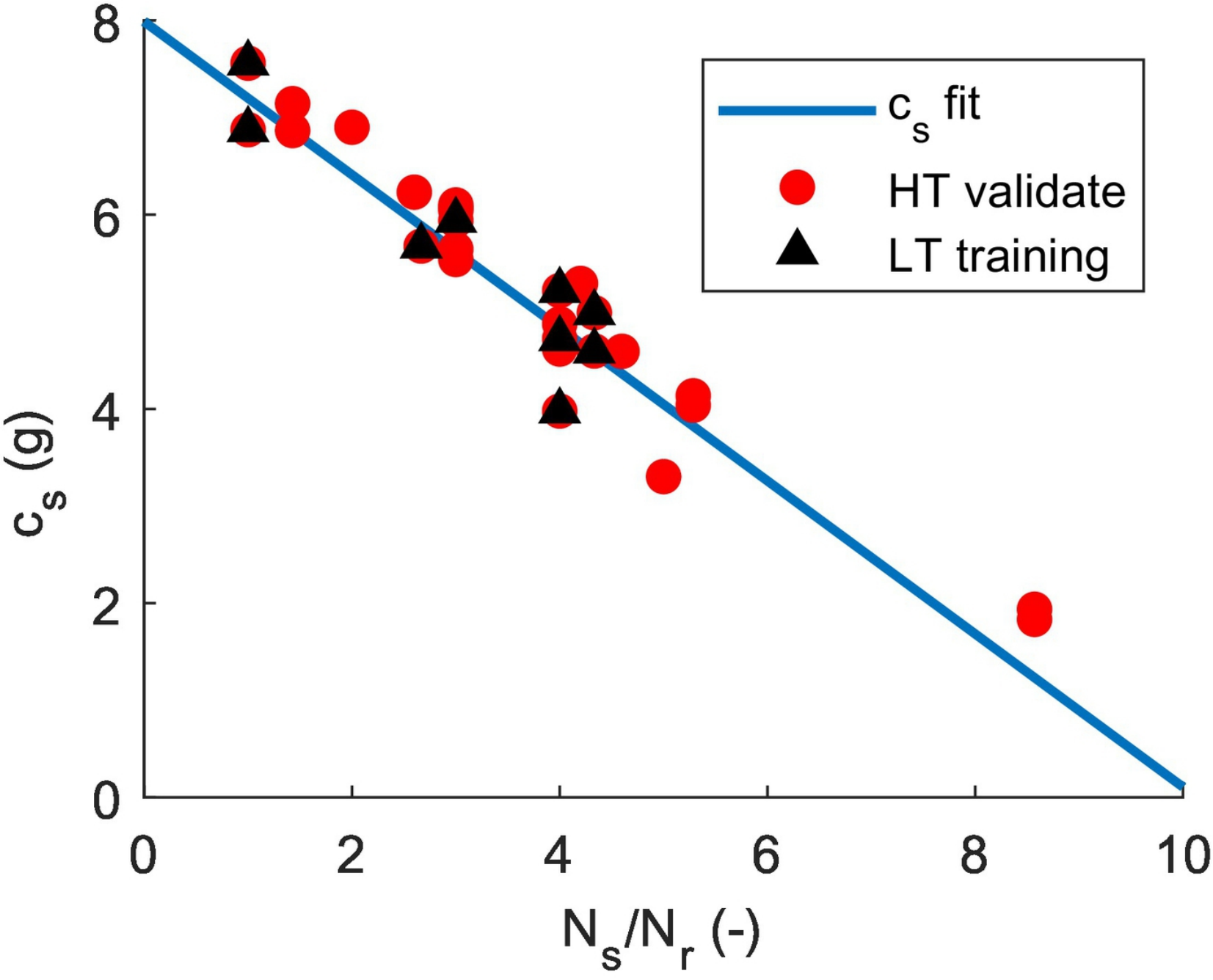

Figure 6

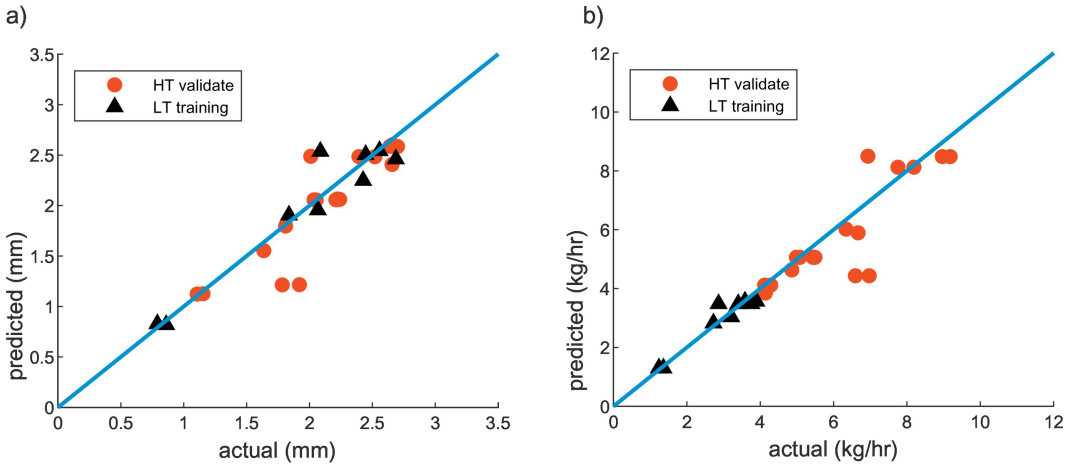
a)
HT validate
LT training
predicted (mm)
actual (mm)
0
0.5
1
1.5
2
2.5
3
3.5
b)
HT validate
LT training
predicted (kg/hr)
actual (kg/hr)
0
2
4
6
8
10
12

Figure 7

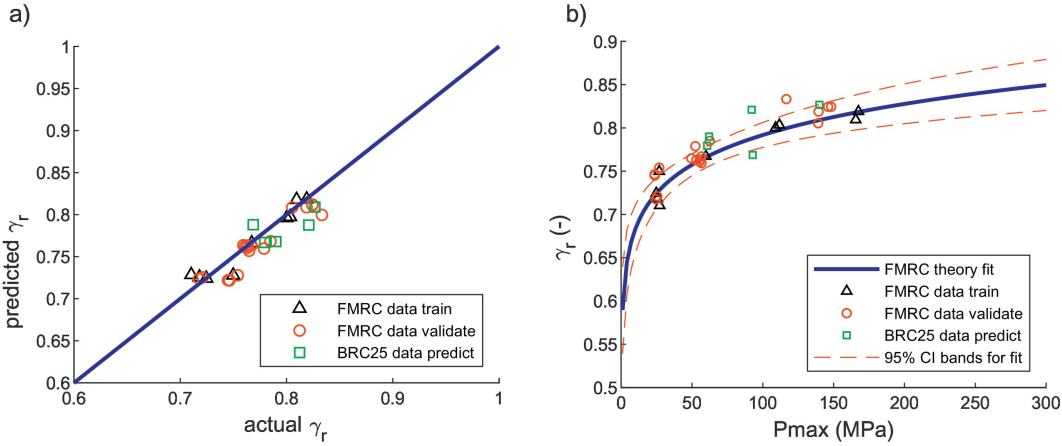
a)
predicted γ_r
actual γ_r
FMRC data train
FMRC data validate
BRC25 data predict
b)
γ_r (-)
Pmax (MPa)
FMRC theory fit
FMRC data train
FMRC data validate
BRC25 data predict
95% CI bands for fit

Figure 8

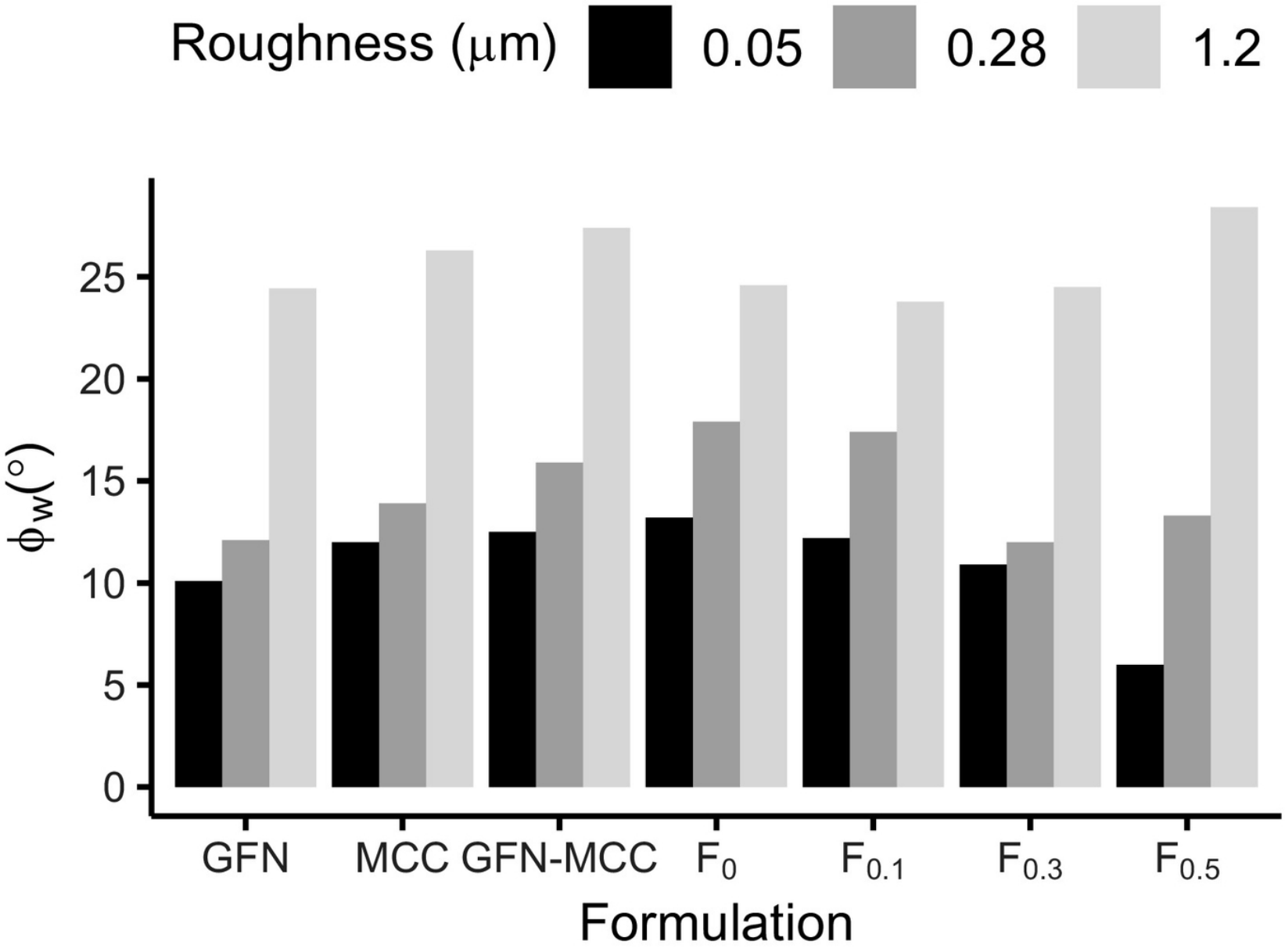
Roughness (μm)
0.05
0.28
1.2
25
20
15
10
5
0
ϕ_w(°)
GFN
MCC
GFN-MCC
F_0
$F_{0.1}$
$F_{0.3}$
$F_{0.5}$
Formulation

Figure 9